An ion-atom merged beams setup at the Cryogenic Storage Ring

F. Grussie,[1, a)] A.P. O'Connor,[1] M. Grieser,[1] D. Müll,[1] A. Znotins,[1] X. Urbain,[2] and H. Kreckel[1,a),b)]
[1)]*Max-Planck-Institut für Kernphysik, Saupfercheckweg 1, 69117 Heidelberg, Germany*
[2)]*Institute of Condensed Matter and Nanosciences, Université Catholique de Louvain, Louvain-la-Neuve B-1348, Belgium*

(Dated: 8 April 2022)

We describe a merged beams experiment to study ion-neutral collisions at the Cryogenic Storage Ring (CSR) of the Max Planck Institute for Nuclear Physics in Heidelberg, Germany. We produce fast beams of neutral atoms in their ground term at kinetic energies between 10 and 300 keV by laser photodetachment of negative ions. The neutral atoms are injected along one of the straight sections of the storage ring, where they can react with stored molecular ions. Several dedicated detectors have been installed to detect charged reaction products of various product-to-reactant mass ranges. The relative collision energy can be tuned by changing the kinetic energy of the neutral beam in an independent drift tube. We give a detailed description of the setup and its capabilities, and present proof-of-principle measurements on the reaction of neutral C atoms with D_2^+ ions.

I. INTRODUCTION

Atomic and molecular collisions are key processes in many disciplines, from fundamental research to cutting edge technological developments. Understanding collision processes on an atomic scale is crucial for astrophysics, atmospheric chemistry and plasma physics. Applications range from nuclear fusion devices to medical treatments and biological imaging. Owing to the relevance of atomic and molecular collisions in those diverse disciplines, a number of experimental methods have been developed for their study throughout the years. One of those experimental methods is the merged beams approach.

Merged beams experiments are typically characterized by two atomic or molecular beams that are guided in such a way that they overlap and propagate in parallel in a straight reaction region, often with nearly-matched velocities. The relative collision energy between the two beam species in the reaction region can be tuned in a controlled fashion by varying one of the beam energies, allowing for energy-resolved studies. The merged beams technique has been applied successfully to investigate a variety of reactions between different atomic and molecular species, among them reactions between neutral atoms[1,2] and atomic ions[3,4] (including highly charged ions[5–8]), ion-ion collisions[9–12], and reactions between neutral atoms and molecular ions[13–17]. Recently, novel methods using magnetic and electric guiding fields for paramagnetic species have enabled ground-breaking experiments on neutral-neutral collisions at very low energies[18,19].

Almost all of the above measurements were carried out in dedicated single-pass experimental setups. Although proof-of-principle experiments were already presented in 1965[20], merged beams have remained a small but important class of experiments in the field of heavy particle collisions. This can be ascribed to technical challenges and a significantly higher level of complexity, when compared to measurements in plasma experiments or drift tubes.

On the other hand, the implementation of merged beams in the field of electron-ion collisions at heavy ion storage rings has been a true success story. Again, the pioneering studies were carried out in single-pass setups[21], however, since their advent in the early nineties, heavy ion storage rings have become the workhorses for electron recombination studies with atomic[22] and molecular ions[23]. Equipped with low-energy electron coolers, several facilities around the world have contributed to an impressive body of work, and demonstrated a remarkable degree of reproducibility[23–25].

One of the main advantages of storage ring experiments with molecular ions lies in the cooling of internal degrees of freedom by spontaneous emission of radiation. For example, many infrared-active molecular ions will relax to their vibrational ground state within the first few seconds of storage, thus allowing for experiments with superior control of the internal energy. The rotational degrees of freedom, on the other hand, were ignored for most of the early studies. As the experiments were carried out in room temperature environments, usually a significant number of rotational states remained populated, even when the molecules had enough time to reach equilibrium with the ambient radiation field. This situation improved dramatically with the introduction of a new generation of cryogenic cooled electrostatic rings, like the Cryogenic Storage Ring (CSR)[26], the RIKEN cryogenic electrostatic ring (RICE)[27], and the double ring facility DESIREE[28] in Stockholm. For both CSR and DESIREE it has been shown that small infrared-active molecular ions like CH^+ and OH^- indeed cool to their lowest rotational states[29–32] within the achievable storage time window.

Combined with a new low-energy electron target, these experimental achievements paved the way for the first quantum-state selective electron recombination studies of HeH^+ at the CSR[33]. It should be stressed that these measurements are not only of great importance for the chemistry of the early universe, they also provide data of a new quality. The state-selectivity – combined with the precise adjustment of the relative collision energy afforded by the merged beams arrangement – enables the determination of energy-dependent recombination cross sections for individual rotational states. These in turn can be convolved with different rotational distributions

[a)]The authors to whom correspondence may be addressed: florian.grussie@mpi-hd.mpg.de, holger.kreckel@mpi-hd.mpg.de
[b)]http://www.mpi-hd.mpg.de/mpi/astrolab

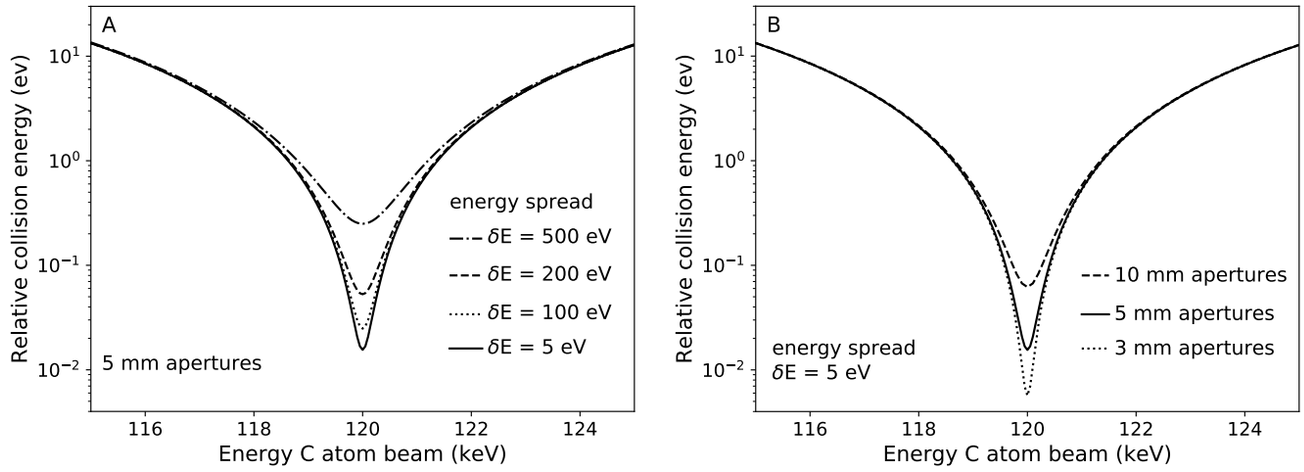

FIG. 1. Outcome of a generic merged beams simulation for the relative collision energy of neutral C atoms colliding with D_2^+ ions. The energy of the D_2^+ beam is fixed at 40 keV, while the energy of the C atoms (given at the x-axes) is modified between 115–125 keV. Panel A shows simulations where the size of the apertures used to collimate the beams is fixed at a diameter of 5 mm, while a Gaussian energy spread between 5–500 eV is assumed for both beams. For Panel B the aperture diameter is varied for both beams, while the beam energy spread is fixed at 5 eV. See main text for details.

and/or kinetic temperatures, and thus be adapted to different environments, without the need for approximations or extrapolations.

Given the success of electron-ion merged beams measurements at storage rings, the possibility of performing ion-neutral merged beams studies at these facilities has been discussed in the community for a long time. However, owing to the difficulties of creating intense and fast neutral beams in well-defined quantum states, no such attempt had been realized thus far. Here we present proof-of-principle results of ion-neutral merged beams measurements carried out at the CSR of the Max Planck Institute for Nuclear Physics in Heidelberg.

II. MERGED BEAMS FOR ION-NEUTRAL COLLISIONS

Compared with the majority of traditional experiments in plasma tubes and afterglows, the merged beams approach has a number of advantages. Its greatest asset may be the fact that it allows for energy-resolved measurements, where the relative kinetic energy of the reactants can be tuned across several orders of magnitude. Furthermore, it often allows for absolute rate coefficient measurements, as the reaction products remain focused and can be detected with near-unity detection efficiency, using modestly-sized single-particle detectors. A full review of the technique and its various applications is beyond the scope of this work, an overview can be found here[34]. In this section a brief outline of the merged beams principle will be given, with special focus on ion-neutral collisions and the implications that the comparatively high beam energies used at the CSR have for merged beams studies.

A general representation of the type of ion-neutral reaction of interest for the present application is

$$\mathrm{A} + \mathrm{M}^+ \longrightarrow \mathrm{X}^+ + \mathrm{Y}\,, \tag{1}$$

where A stands for a neutral atom and M^+ denotes a positively charged molecular ion, whereas X^+ and Y denote charged and neutral reaction products, respectively.

The relative collision energy in the center-of-mass frame for two non-relativistic, intersecting particle beams with kinetic energies E_1, E_2 and masses m_1, m_2, respectively, is given by

$$E_r = \frac{1}{2}\mu v_r^2 = \mu\left[\frac{E_1}{m_1} + \frac{E_2}{m_2} - 2\left(\frac{E_1 E_2}{m_1 m_2}\right)^{\frac{1}{2}}\cos\theta\right], \tag{2}$$

where v_r denotes the relative velocity and μ the reduced mass ($\mu = m_1 m_2/(m_1+m_2)$). Let's assume an idealized experiment with perfectly collinear merged beams ($\cos\theta = 1$) and energies for both beams chosen such that $E_1/m_1 = E_2/m_2$ (corresponding to equal beam velocities), then the terms in the square brackets cancel and it follows that $E_r = 0$. Thus, in an ideal world, it is possible to have two beams of different masses interact at nominal zero collision energy in the center-of-mass frame. In reality, the velocity match is never perfect, and – more importantly – the angular divergence of the beams and the energy spread of the ion sources will induce a finite resolution limit at low collision energies.

In Sect. V we will present proof-of-principle results for the reaction

$$\mathrm{C} + \mathrm{D}_2^+ \longrightarrow \mathrm{CD}^+ + \mathrm{D}\,, \tag{3}$$

and additional data on collisions of C atoms and H_2D^+ ions will be published in a forthcoming article[35]. Thus, without any loss of generality intended, we will base most of our quantitative considerations and simulations on these examples.

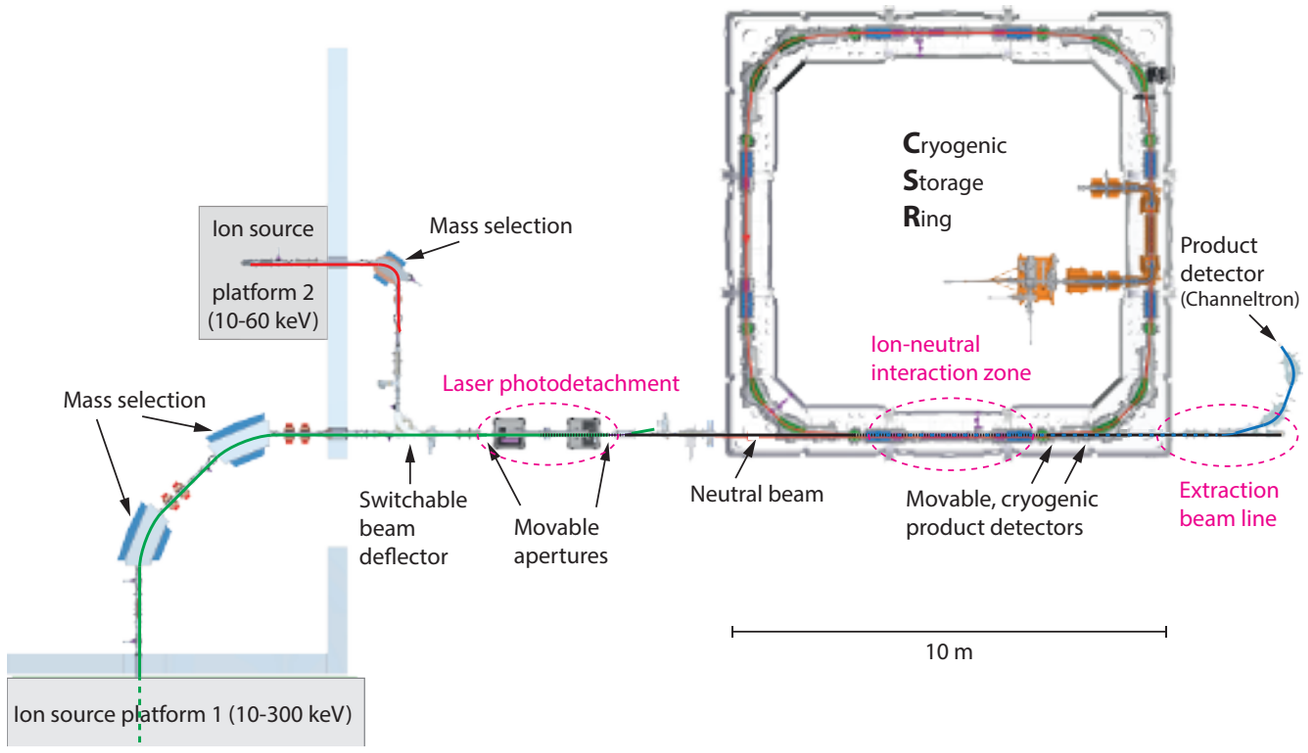

FIG. 2. Overview of the Cryogenic Storage Ring and the infrastructure and peripherals relevant to the ion-neutral experiment. Note that only a small part of source platform 1 is shown here for completeness. Details on the sections that have been developed specifically for the ion-neutral experiment (like, e.g., the photodetachment region and the extraction beam line) are given later in the text.

The CSR can store particle beams with kinetic energies of up to 300 keV per unit charge, and using beam energies below 30 keV for singly charged ions typically affects the quality of the stored beams negatively and leads to reduced lifetimes. As a consequence, our experiments require somewhat larger kinetic energies for both beams when compared to most previous single-pass merged beams studies between neutral atoms and molecular ions[15–17]. To examine the systematic influence of beam size and energy spread at these energies, we have made generic Monte-Carlo simulations to calculate relative collision energies for the deuterium abstraction reaction given in equation (3), the outcome is shown in Figure 1 (note that these general calculations are only for illustrative purposes on merged beams dynamics, detailed and specific simulations for the CSR setup will be presented in Sec.IV). We assume that the D_2^+ beam has a fixed kinetic energy of 40 keV, while the energy of the C beam is varied between 115–125 keV. Both beams are collimated by circular apertures of the same diameter, which are 2.9 m apart. The relative collision energy of the merged beams is simulated for a 1 m long interaction zone starting immediately behind the second aperture. A Gaussian energy spread – representing a distribution of kinetic energies caused by the ion source and acceleration stages – is assumed for both beams. We varied the aperture size between 3 mm and 10 mm, and the energy spread from 5 eV to 500 eV. Note that the plots show only the *average* of the relative collision energies that we inferred from the simulation, in order to illustrate the dependence on beam collimation and energy spread. The experimental resolution also depends on the distribution of the relative collision energies and specific simulations for the CSR setup will be addressed at a later stage.

Typical energy spreads for standard ion sources (e.g., duoplasmatron or discharge sources) are on the order of 10 eV[5,36] and they can have a major influence on the center-of-mass collision energies when measuring at lower beam energies. However, for the energy range that is pursued in the present experiments, such an energy spread would have a minor influence on the average collision energy. As the data in Panel A of Fig. 1 shows, clear deviations at the lowest relative collision energies begin to show up for beam energy spreads on the order of 100 eV. In fact, for the simulations shown here – which assume an aperture diameter of 5 mm – energy spreads with $\delta E < 30$ eV are not distinguishable. Nevertheless, broader energy distributions can occur during the acceleration of the beams, caused by voltage fluctuations of the acceleration stages or ion optics. Our simulations show that it is important to keep these effects at a minimum.

Arguably the more important parameter, however, proves to be the angular divergence of the beams. Panel B shows that the achievable minimal collision energy increases by more than an order of magnitude, when the collimation of the beams is changed from 3 mm to 10 mm. While stronger collimation is always preferable in terms of resolution, it usually goes at the expense of signal strength, as smaller apertures translate into lower currents. For the design of the merged beams setup at the CSR, it was particularly challenging to find the optimal

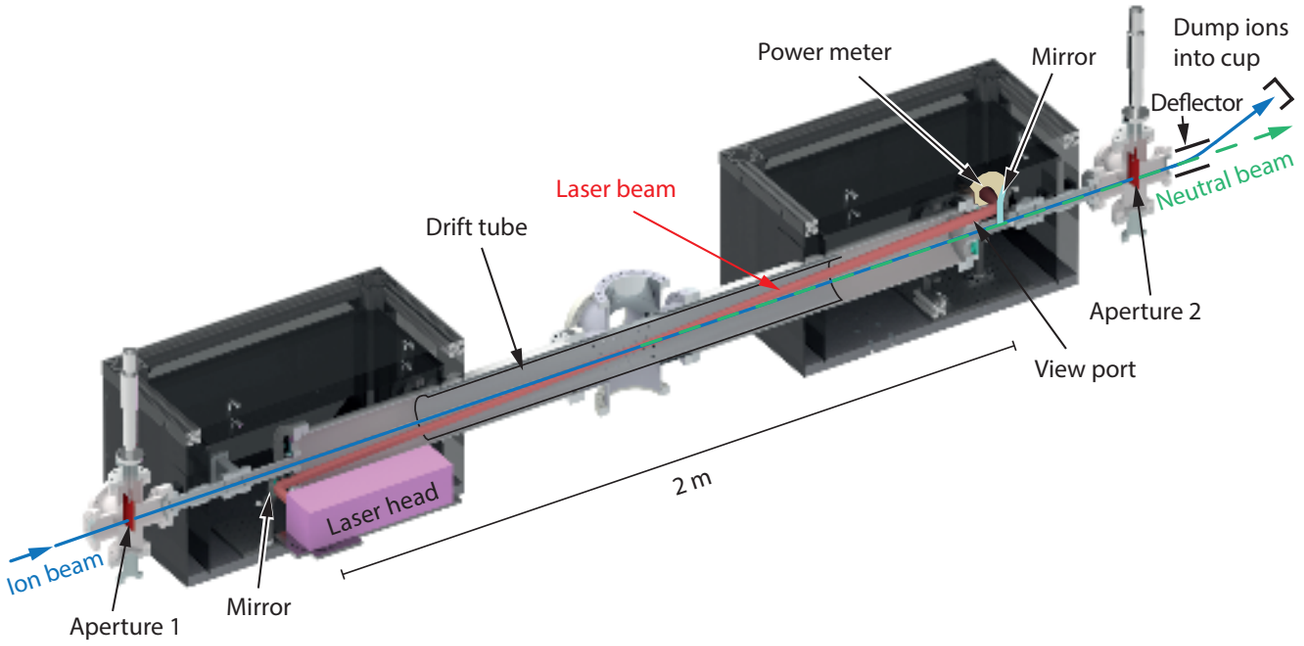

FIG. 3. Sketch of the photodetachment section. The light from the 2 kW diode laser array (operating at a wavelength of 808 nm) is coupled into the vacuum chamber through anti reflection-coated viewports and superimposed to the ion beam at an angle of 2.7°. Photodetachment takes place in a drift tube that can be used to accelerate and decelerate the anions prior to neutralization and thus modify the kinetic energy of the neutral beam. At the laser exit port the laser beam is deflected into a water-cooled power meter to monitor the power level continuously. Note that in the present configuration the laser beam intersects the ion beam in the vertical plane, contrary to previous designs[37]. The changed geometry accounts for the fact that the laser profile in the central focus area is narrower in the vertical direction and thus the photodetachment efficiency can be improved considerably.

balance between signal strength and resolution, as we had to take into account the restrictions imposed by the size and ion optical lattice of the storage ring.

III. EXPERIMENTAL SETUP

A. Overview

Figure 2 shows an overview of the Cryogenic Storage Ring and the infrastructure that is relevant to the merged beams experiment. The storage ring has a circumference of 35.12 m. With its electrostatic ion optics, the CSR can store positive and negative particles with up to 300 keV kinetic energy per unit charge (details on the storage ring parameters and capabilities can be found in a dedicated review[26]). The CSR has a nested vacuum structure with large outer cryostat chambers and inner ultra-high vacuum chambers, which can be cooled to cryogenic temperatures (∼5 K) by a closed-cycle liquid helium circuit. The inner vacuum chambers also house the high voltage electrodes that keep the stored particles on a revolving orbit.

The overall shape of the particle orbit inside the CSR is defined by cylindrical dipole deflectors, with each storage ring corner housing two 39° deflectors and two 6° deflectors. Two quadrupole doublets are situated in each straight section between the dipole deflectors for focusing, amounting to a total of eight quadrupole doublets organized in four independent families. The ion optical lattice is important for the layout and placement of the product detectors and will be discussed in more detail later.

Two high voltage platforms are used to supply fast ion beams to the CSR. The main ion source platform can be operated with voltages up to 300 kV, and it is large enough to accommodate several types of ion sources at the same time. Since the merged beams experiment requires two different ion beams simultaneously, a second high voltage platform was constructed. The second platform is significantly smaller in size (note that only a small part of source platform 1 is shown in Figure 2), and its layout allows for the installation of only one ion source with a maximum platform voltage of 60 kV. Either platform can be used to deliver both positive and negative beams to the CSR. In the transfer beam line a large 90° deflector with a hole in its outer electrode is used to switch between the platforms. The deflector is equipped with fast high voltage switches which permit us to change between the ion beams within sub-milliseconds. Most of the ion optical elements in the transfer beam line downstream from the 90° deflector can also be switched, to adapt the beam optics to the type of ion beam coming from either platform.

The neutral beam for the merged beams experiment is produced by laser photodetachment of a negative ion beam. In principle it would have been possible to have a dedicated negative platform just for neutral beam creation, and to inject the

neutral beam into any of the straight sections of the CSR. In this scenario the main ion source platform would always be used to provide the ions to be stored inside the CSR. However, since the construction of another 300 kV platform for the neutral beam would have been prohibitive in terms of cost and size, this approach would have limited the energy of the neutral beam severely. To achieve maximum flexibility for the choice of ion- and neutral beam energies, we decided to use the straight section downstream of the main transfer beam line for the merged beams experiment, allowing us to use either platform for ion injection into the CSR or neutral beam preparation, depending on the mass of the reactants.

B. Neutral beam creation and characterization

We create the neutral atoms by partial laser neutralization of a negative ion beam, largely following the example used in previous single-pass experiments[4,36] and described in detail here[37]. The photodetachment section is situated in the CSR transfer beam line (see Fig. 2), upstream from the straight section of the CSR that is used for ion injection. The laser system consists of an array of high power diode lasers, operating at a wavelength of 808 nm. The diodes are arranged in two stacks with 15 diode bars each and 19 emitters per bar. The beams from the two laser stacks are merged by interleaved mirrors and coupled in- and out of the vacuum chamber by anti reflection-coated viewports. To improve the photodetachment efficiency the laser is superimposed to the ion beam at a grazing angle of $\theta = 2.7°$, effectively extending the overlap between laser and ion beam by a factor $1/\sin\theta \approx 20$, when compared to a crossed-beam arrangement at right angles. To adapt the overlap geometry better to the laser profile, in our setup the laser beam intersects the ion beam in the vertical plane, contrary to previous implementations[37]. Since the laser profile around the focus area is narrower in vertical direction, this configuration is expected to increase the photodetachment efficiency by a factor of $\sim$1.68[37]. The laser system is specified to run at a continuous power level of up to 2 kW, but it can also be switched on and off at frequencies of up to several kHz.

Two apertures with a diameter of 4.5 mm each are placed upstream and downstream of the photodetachment chamber (apertures 1 and 2 in Fig.3). These apertures are used to collimate the neutral beam, and they are carefully aligned by telescope to the central axis of the CSR injection section. The aperture diameter is chosen such that none of the neutralized particles that travel through both apertures in a straight trajectory can be lost inside the CSR; in fact, all of the neutrals that pass through the CSR unperturbed will be captured in a large dedicated cup situated at the end of the CSR extraction section. The apertures can be moved out pneumatically for each particle injection into the CSR to maximize the number of stored particles, however, we found that for most measurements with strong ion sources we can leave the apertures in and still have enough ions to fill the storage ring.

The neutralization takes place inside a voltage-adjustable drift tube situated inside the photodetachment section (see Fig. 3), which can be biased by voltages U_{drift} of up to $\pm$5 kV. The negative ion beam at kinetic energy E_{neg} that enters this drift tube region will be accelerated (for positive drift tube voltages) or decelerated (for negative voltages) upon entry, and it will be returning to its original kinetic energy when exiting the drift tube. Those atoms that are neutralized inside the drift tube, however, will remain at the altered energy of $E_{\text{neg}}+eU_{\text{drift}}$. Thus, by changing the drift tube voltage we can tune the neutral beam energy without having to re-align the injection beam line. Figure 4 shows the relative collision energy for collisions of a 40 keV D_2^+ beam interacting with a neutral C beam at initial energies of 122 and 118 keV, for the full range of the drift tube voltage. Obviously, we can scan the same relative collision energies either with the D_2^+ beam being faster or slower than the C beam. In the experiment, we typically realize both scan directions for a cross-check of the experimental parameters.

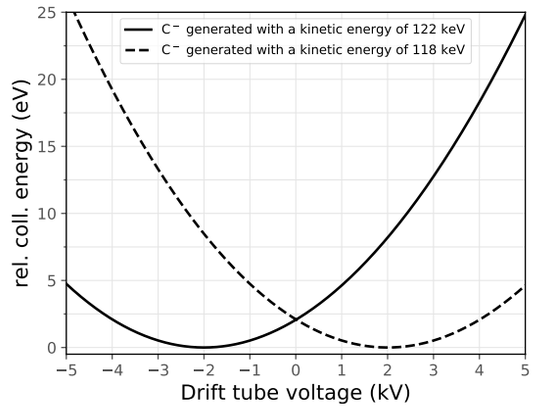

FIG. 4. Calculated relative collision energy as a function of the drift tube voltage for D_2^+ with a kinetic energy of 40 keV stored inside CSR, while the kinetic energy of the merging C atoms is varied according to 122/118 keV + eU_{drift}, respectively.

In principle, it would also be possible to vary the relative collision energy by tuning the energy of the stored ion beam. A drift tube inside the overlap region of the storage ring is available for this purpose. However, our simulations have shown that the use of this drift tube would complicate the measurements significantly, as the fields would lead to a focusing effect (similar to an Einzel lens). This would result in a modification of the effective overlap during an energy scan, and the fringe fields created by the drift tube would lead to additional smearing of the relative collision energies. Furthermore, the tune of the storage ring would change, with adverse effects on the lifetime and the emittance of the stored ion beam. While the drift tube inside the CSR may become useful for certain measurement schemes in the future, the current operation mode, where we modify the neutral beam energy by tuning a drift tube in the injection section, is much more straightforward.

Behind the photodetachment section a switchable parallel-plate deflector is used to guide the remaining ions into a Faraday cup, where the ion current can be recorded continuously.

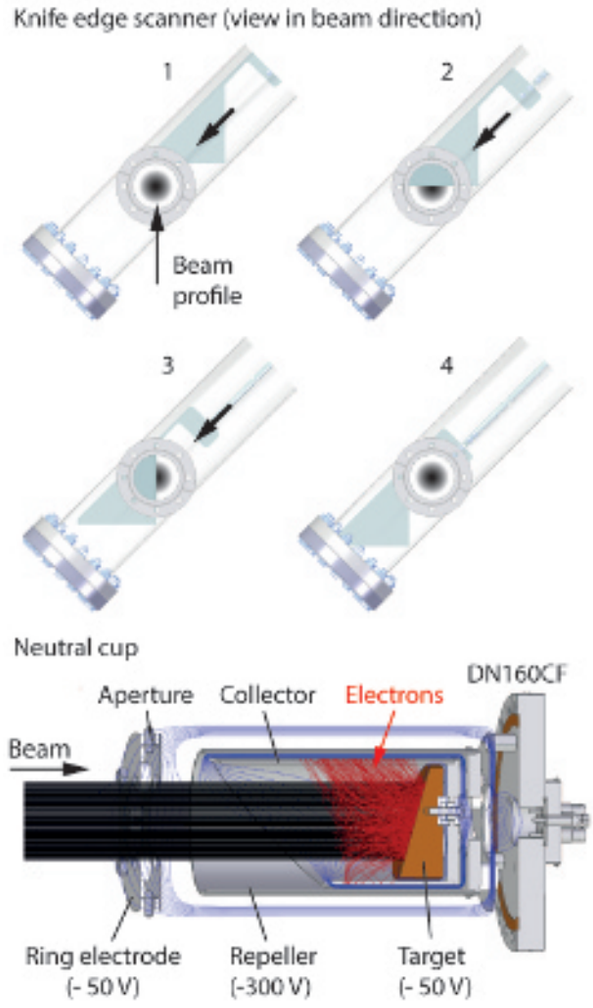

FIG. 5. Sketch of the neutral cup that is used to measure the flux of neutral atoms at the end of the CSR extraction section (lower panel). The measurement principle relies on secondary electron emission upon impact of the neutrals on a copper target. Repeller and target electrodes are biased to make sure all electrons are collected. The red traces represent a SIMION simulation of the secondary electron trajectories. The upper panel shows the movable knife-edge scanner that is installed in front of the cup. By moving a triangular shape in front of the cup, and at the same time recording the variation in the signal, caused by the change in the effective cross sectional area of the cup, the horizontal and vertical beam profiles can be determined (see main text for details).

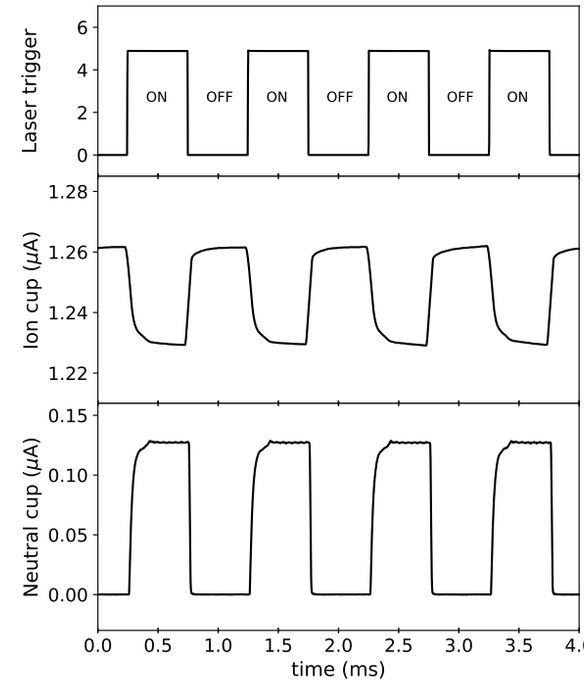

FIG. 6. Comparison of the currents measured in the ion and neutral cups during laser switching. The signal in the ion cup is somewhat distorted by the capacity of the Faraday cup, while the signal in the neutral cup represents the actual temporal evolution much better (see main text for details). The measurements were made with a 122 keV C^- beam. The laser was operated with a diode current of 80 A (corresponding to a power level of 1.8 kW during the laser-on phases) and switched on and off at a frequency of 1 kHz. The average loss in the ion current during the laser-on phase can be used to determine the photodetachment efficiency, which at this comparatively high beam energy corresponds to 2.4 %. Note that the current measured in the neutral cup corresponds to the flux of neutral atoms multiplied by the average yield of secondary electrons per neutral impact, which can vary, depending on the beam energy and the surface condition of the target inside the neutral cup.

At the same time the neutral flux is measured in a dedicated cup situated at the end of the CSR extraction section. This neutral cup (Fig. 5) has a large acceptance diameter of 75 mm and it measures a signal proportional to the neutral flux by collecting the secondary electrons emitted from a copper surface upon particle impact. Careful design of the collector electrodes was necessary to make sure all electrons are collected, while at the same time preventing unwanted background from stray charge carriers inside the vacuum chamber[38]. By connecting the target and collector electrode, the cup can also be used as an ordinary Faraday cup to measure ion beam currents. The signal of both cups is amplified by low noise current amplifiers (FEMTO DLPCA-200) and fed into the data acquisition system via analog-to-digital converter cards.

Figure 6 shows signal traces for both cups during laser switching with 1 kHz, using a C^- ion beam at 122 keV kinetic energy. The photodetachment efficiency can be derived from the reduction in the ion current during the laser-on-phases. In this case we infer an efficiency of 2.4 %, in agreement with previous calibration measurements at lower energies[38], which have to be scaled with the inverse of the ion velocity, as a measure of the dwell time of the ions inside the laser field. The signal in the neutral cup is given by the flux of neutral particles multiplied with the so-called γ-factor, representing the average yield of secondary electrons per neutral impact. The exact value of γ depends on the type and velocity of the neutral particles, as well as the surface conditions of the target electrode. Therefore it has to be determined anew for each mea-

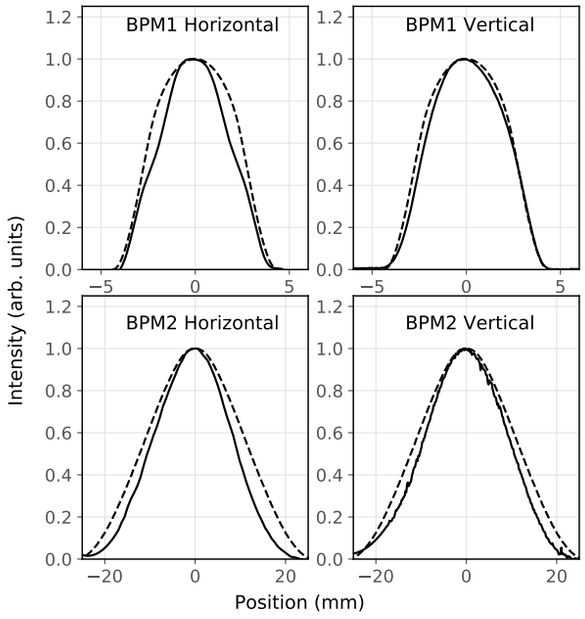

FIG. 7. Examples of neutral beam profiles. The solid lines show horizontal and vertical profiles recorded at the wire scanner in the transfer beam line (upper panels) and the knife-edge scanner situated in the extraction section, downstream of the CSR (lower panels). The dashed lines show a simple geometric simulation of the neutral beam (see text for details).

surement (especially if the chamber was vented and exposed to air). As long as the Faraday cup is kept under vacuum and the impact position of the beam on the target remains stable during a measurement campaign, the γ factor typically varies by less than 15%.

Note that the signal for the ion cup shown in Fig. 6 is somewhat distorted, as the capacity of the cup, in combination with the bandwidth of the current amplifier, softens the flanks (we have verified that the plateau at the end of the laser-on phase is reached, by using longer switching times). The signal in the neutral cup represents the temporal evolution much better. When the laser is switched on, the power level increases quickly (rise time on the order of $20\mu s$, verified with a photodiode), but it takes a little longer until the full power level is reached. This is not a problem for the ion-neutral measurements, as we typically operate at a slower switching rate, with 15 ms time steps. Since the neutral cup signal is also less prone to electronic noise, we usually use the neutral signal for the data analysis, and calibrate it using the γ factor that we average over several measurement runs.

The shape of the neutral beam is mainly determined by the two apertures that collimate the beam, as they strongly limit the beam emittance. We use two beam profile monitors (BPMs) outside the CSR to verify that the beam remains centered. A commercial wire scanner (National Electrostatic Corporation BPM82) is located in the CSR injection section. Typical profiles recorded with this device are shown in the upper panel of Fig. 7 together with a simulation of the neutral beam, which assumes that the emittance of the negative ion beam is much larger than the emittance selected by the collimation apertures, and thus the beam covers the apertures homogeneously. While the vertical profiles agree very well, the horizontal profile shows that the transmitted beam is slightly narrower than the simulation. To determine the beam shape behind the CSR is more challenging. Since the neutrals at this point have flown ballistically for more than 15 m, the beam is much wider and the density is too low for standard scanners. We have built a dedicated knife-edge scanner that consists of a metal blade that is moved slowly through the beam pipe in front of the neutral cup (see Fig. 5). The measurement principle is similar to that of optical knife-edge scanners, routinely employed to determine laser beam profiles[39,40]. Moving a triangular shape in front of the cup, while continuously recording the cup signal, allows us to record the horizontal and vertical profiles separately, however – owing to the small neutral beam density – this procedure requires averaging for best results and one full scan takes about 15 min. The lower panels of Fig. 7 show exemplary horizontal and vertical profiles obtained with this second scanner inside the extraction beam line.

We typically find that the neutral beam almost fills the apertures and thus agrees with an emittance-limited simulation of a ballistic beam propagation. If the beam shows irregularities in its shape, they have to be within the limits prescribed by the apertures, and the fitted beam center typically deviates by less than 2 mm from the calibrated zero position at the position of the second BPM, thus limiting the average angle between neutral beam and the nominal axis of the CSR in the injection section to less than 0.15 mrad. In summary, our simulations in the next sections will show that the position and alignment of the ion beam inside the ring poses a much greater limitation for our measurements than the neutral beam.

C. Product detection

All reactions of interest for the present experiment result in one neutral and one charged reaction product, according to Eq. 1. The neutral product Y will usually be embedded inside the neutral beam, and while the detection of neutral products may be possible for certain reactions and dedicated setups[4], we exclusively pursue the detection of the charged reaction products X^+ for the CSR experiments, as it is much more straightforward. In general, the first 6° deflector behind the ion-neutral interaction zone will deflect the charged products and introduce an angle with respect to the neutral beam. Depending on the mass ratio of the X^+ daughter product compared to the initial ion beam M^+, stored inside the CSR, this deflection may leave the X^+ products on a trajectory between the neutral beam and the stored ions (for $m[X^+] > m[M^+]$), or the charged products may be deflected even stronger than the stored ion beam toward the center of the CSR (for $m[X^+] < m[M^+]$).

To cover different scenarios and mass ratios, we installed three single particle detectors, dedicated to the ion-neutral experiment. The first two detectors are situated inside the storage ring, in two chambers downstream of the second 6° deflec-

tor in the ion-neutral interaction section. These detectors are based on micro-channel plates (MCPs) that detect secondary electrons emitted from converter plates following ion impact. The design resembles the detectors developed for the electron cooler section[41,42], however, for the present experiment the open area has been increased significantly to $48 \times 55\,\mathrm{mm}^2$, and a harp made from stainless steel wires and biased with a negative voltage to repel low-energy electrons has been introduced. Both detectors can be operated at cryogenic temperatures, and they are movable on rails inside the experimental vacuum chambers. To increase the detection efficiency and reduce dead times, the MCPs are typically heated with $\sim$100 mW during operation, by small heating coils situated at their support base.

Figure 8 shows an overview of the CSR section downstream of the ion-neutral overlap region. The positions of the two movable detectors and the accessible mass ranges $m[X^+]/m[M^+]$, based on trajectory simulations, are given. Note that these mass ratios depend heavily on the size and emittance of the stored ion beam, and the numbers given here are meant as guidelines only. They are based on simulations using typical values for beam size and emittance of an uncooled ion beam. One of those trajectory simulations is shown in the middle panel of Fig. 8, depicting the example reaction $HeH^+ + D \longrightarrow HD^+ + He$. The lower panel shows simulations for the reaction $D_2^+ + C \longrightarrow CD^+ + D$, which results in a charged product that is much heavier than the initial ion beam. The simulation shows that the products do not fully separate from the neutral beam inside the CSR vacuum chambers. In fact, for mass ratios $m[X^+]/m[M^+] > 3.2$, the product and the neutral beams generally tend to overlap inside the CSR. Therefore, we have installed a parallel plate deflector toward the CSR extraction beam line. This deflector permits us to bend heavy charged fragments back into the neutral beam and analyze them outside of the CSR using a series of deflectors and two energy-analyzing 55° deflectors (see Fig. 9), followed by a channeltron detector. This arrangement also allows for more detailed analysis of the reaction products. Using movable slits between the two 55° deflectors, we can discriminate between various charged reaction products. Figure 9 shows a simulated outcome of the reaction $H_2D^+ + C$, where we have selected the CD^+/CH_2^+ reaction channel, while all products of a different mass are stopped before the slits.

We have performed extensive simulations using both MAD-X[43] and G4beamline[44] codes (for which the field maps of the ion optical elements were calculated with TOSCA Opera3D[45]) to optimize all voltages for the deflectors in the extraction beam line to a given product energy, taking into account the change of the neutral beam energy induced by the drift tube voltage in the photodetachment section. Owing to our comparatively high beam energies, we neglected the kinetic energy release at this stage. Note that the product ions inside the extraction beam line are not only deflected, but also focused by the quadrupole doublet close to the entrance of the beam line, which increases the detection efficiency substantially. We benchmarked our simulations with a mono-energetic C^+ ion beam that we transmitted through the extraction beam line. Moreover, during the initial ion-neutral

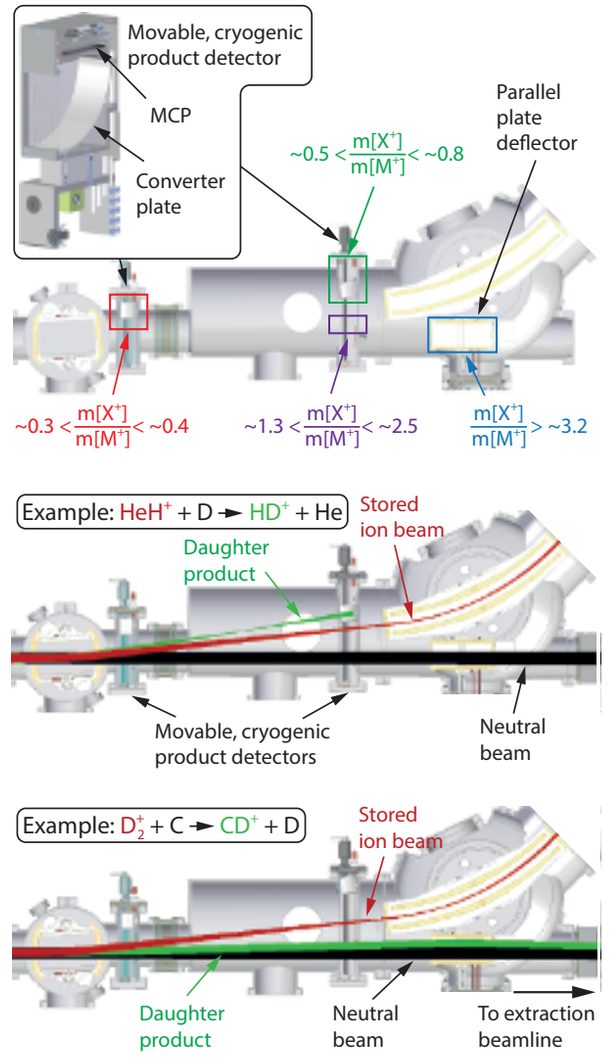

FIG. 8. Schematic drawing of the storage ring section downstream of the ion-neutral overlap region. The particle trajectories in this section are relevant for the product detection. Two movable cryogenic detectors can be used to detect charged reaction products. The approximate mass detection range of the reaction product (mass $m[X^+]$) compared to the mass of the stored ion beam (mass $m[M^+]$) is given in the insets of the upper panel. The middle panel shows exemplary trajectories for the reaction $HeH^+ + D \longrightarrow HD^+ + He$. The lower panel depicts the reaction $D_2^+ + C \longrightarrow CD^+ + D$. As can be seen, for $m[X^+]/m[M^+] > 3.2$ the reaction products and the neutral beam do not fully separate inside the CSR chambers. Therefore, the products are deflected back into the neutral beam by a parallel plate deflector and eventually analyzed by two large electrostatic energy filters outside of the storage ring (see main text for details) .

experiments we varied all deflector voltages individually, and found that the simulated voltages yielded the maximum count rate, indicating that the optimization was successful.

In the meantime, we have successfully used the mass-separating capabilities of the extraction beam line to measure branching ratios, and we will report the results in a forthcoming article[35].

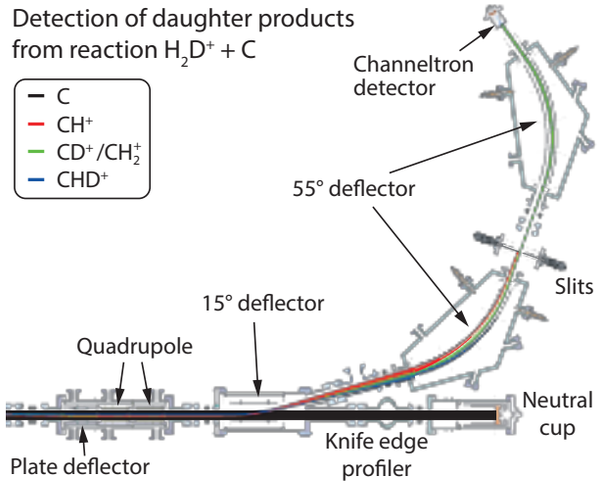

FIG. 9. Schematic drawing of the CSR extraction beam line together with simulated particle trajectories of the daughter products of the ion-neutral reaction H_2D^+ + C. In this simulation the potentials of the ion optical elements in the extraction beam line are scaled in order to detect the CD^+/CH_2^+ products. In this case, the two 55° deflectors (acting as energy filters) allow for the separation of the daughter products into three channels: CH^+, CD^+/CH_2^+, and CHD^+.

IV. SIMULATION OF THE MERGED BEAMS OVERLAP AND THE COLLISION ENERGY DISTRIBUTION

To assess the effective overlap between ions and neutrals and the energy resolution of the experiment, detailed simulations of the trajectories of the stored ions and the resulting overlap with the neutral beam were carried out. A crucial parameter for merged beams studies is the overlap factor Ω[36]

$$\Omega = \frac{\int\int\int J_{M^+}(x,y,z)J_A(x,y,z)dxdydz}{\int\int J_{M^+}(x,y)dxdy \int\int J_A(x,y)dxdy}, \quad (4)$$

where J_{M^+} and J_A denote the fluxes of the stored ion beam and the neutral atom beam, respectively. We introduce a Cartesian coordinate system (x,y,z), where the z-axis is collinear with the central axis of the neutral beam (and thus the nominal ion beam orbit in the center of the CSR injection section), the x-coordinate points toward the center of the storage ring, and the y-coordinate points upward, perpendicular to both x- and z-axes. Following the argumentation in[36], we can define the overlap along the z-axis by

$$\Omega(z) = \frac{\int\int\int J_{M^+}(x,y,z)J_A(x,y,z)dxdy}{\int\int J_{M^+}(x,y)dxdy \int\int J_A(x,y)dxdy}, \quad (5)$$

and define an average value over the entire length L of the interaction volume

$$\langle\Omega(z)\rangle = \frac{1}{L}\int \Omega(z)dz. \quad (6)$$

With the shape of the neutral beam severely constrained through the apertures in the photodetachment region, the size and divergence of the ion beam in the interaction section become the essential parameters to determine the value of $\langle\Omega(z)\rangle$. The simulations of the trajectories of the stored ions were carried out with the G4beamline code. Precise field maps for all ion-optical elements were created using the finite-elements code TOSCA[45]. Exact geometrical models for all elements were used and discretized on a three-dimensional mesh.

The upper panel of Figure 10 shows simulated trajectories for both ion and neutral beam in the interaction section. While the neutral beam simply expands ballistically, the ion beam passes through both deflecting and focusing elements in this section. The deflecting elements are the two 6° deflectors, which effectively merge and de-merge the beams, while the focusing action is caused by the two quadrupole doublets situated in each straight section of the CSR, as part of the symmetric ring lattice. Details on the CSR ion optical layout can be found in[26].

Simulations for the standard CSR working point and two realistic ion beam emittances are used to extract the overlap value along the interaction section in the lower panel of Fig. 10. The smaller 2σ-emittance value of 5 mm mrad is unrealistic for an un-cooled coasting beam (when having a high number of stored ions inside CSR), but it is a reasonable estimate for future experiments where the CSR electron cooler is applied for translational cooling. In principle, the two apertures in the transfer beam line from the ion source to the CSR limit the 2σ-emittance of the transported beam to ∼1.4 mm mrad, however, due to intra-beam scattering and imperfect matching of the transfer beam line to the storage ring Twiss parameters at injection, we often observe in our experiments that the stored ion beam occupies a larger phase space. From imaging studies we inferred a value of $\varepsilon_{x,y}(2\sigma)$∼10 mm mrad as a typical value for an uncooled ion beam, when storing $\sim 10^8$ particles inside CSR.

The overall decrease of $\Omega(z)$ along the beam axis is owed to the decrease of the neutral beam density because of its ballistic expansion. The shaded areas inside the graph depict the location of the quadrupole doublets and 6° deflectors, according to the legend in the inset. The average values for the integrated overlap $\langle\Omega(z)\rangle$ range between 0.35 and 0.43 cm^{-2}, however, the lower value is probably closer to reality for the present proof-of-principle measurements with an un-cooled beam and no particular efforts to match the storage ring parameters at injection.

Figure 11 shows the resulting collision energies for both ion beam emittances. The color coding divides the events in three regimes, depending on where in the interaction region they occur. The blue area shows all events stemming from collisions in the straight section between the quadrupoles. These are the majority of events and the ones with the lowest average collision energy. The dashed lines show a fit with a Maxwell-Boltzmann velocity distribution with a mean energy expressed in k_BT, ranging from 0.033 to 0.063 eV for the two different emittance values. The area shaded in yellow is caused by the merging and de-merging of the beams in the 6°-deflectors. The large angle between the two beams in these sections results in very high relative collision energies, exceeding 100 eV in this case. Since the cross sections that we aim to study usu-

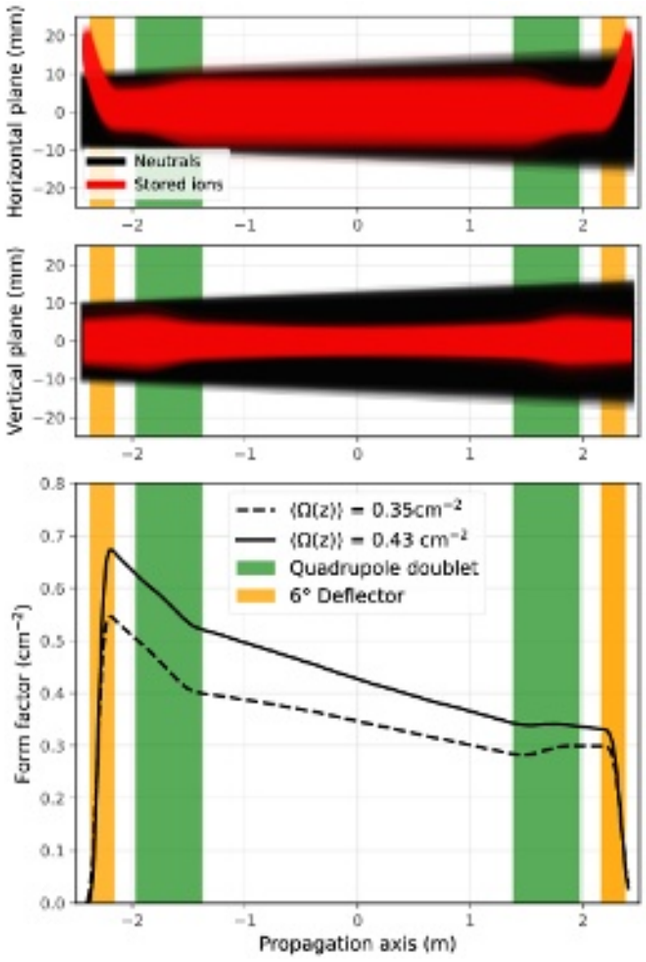

FIG. 10. The upper two plots show the trajectories of a neutral beam (black lines) and a stored ion beam (red lines) with an emittance of $\varepsilon_{x,y}(2\sigma)$ = 5 mm mrad, projected onto the horizontal and vertical plane, respectively. The lower diagram shows the calculated overlap form factor along the propagation axis in the CSR interaction section: for a stored ion beam (in CSR standard mode) with an emittance of $\varepsilon_{x,y}(2\sigma)$ = 5 mm mrad (black line) and for a stored ion beam with an emittance of $\varepsilon_{x,y}(2\sigma)$ = 10 mm mrad, merged with a neutral beam collimated by 4.5 mm apertures in the injection beam line.

ally tend toward zero at these high collision energies, and the fraction of events in this area is low (on the order of 2%), we can assume that our measurement will not be affected significantly by the events in the deflectors. Moreover, our simulations show that when collisions occur in the deflectors, the angle between the two beams is often so large, that only a fraction of those events will be transmitted through our energy analyzers and end up at the detector. The situation is different for the collisions taking place in the quadrupoles, which are shaded in green. The focusing fields in these ion optical elements will introduce an angle between the ion and neutral beams, also leading to higher collision energies.

The simulated collision energy distribution can be used to correct the experimental data and account for the increased collision energies in the focusing sections. However, owing to the smooth shape of the rate coefficient for the C + D_2^+ reaction, combined with the sharp drop at higher energies (shown in Sect. V C), the correction turned out to have a minimal effect on the shape of the curve for our proof-of-principal data, while it would have increased the overall value by about 15%. Since for the present work we do not aim at a measurement of an independent rate coefficient on an absolute scale, but rather a calibration of our measured proof-of-principle data to previous studies, we will present our data without correction.

V. EXPERIMENT: C + $D_2^+ \longrightarrow CD^+ + D$

Here we report on energy-resolved measurements of Reaction 3, carried out with the CSR ion-neutral collision setup.

The D_2^+ ion was chosen as a reactant for these benchmark measurements for two reason: firstly, because two independent and absolute previous single-pass merged beams studies exist to calibrate our results[14,46]; secondly, because the D_2^+ ion does not possess a dipole moment, and therefore its internal excitation will not change during storage inside the CSR. Moreover, the distribution of vibrational and rotational states populated in D_2^+ ions created by electron-impact in conventional ion sources is well-studied and believed to be reproducible. Consequently, comparisons between previous single-pass studies and our storage ring measurements become meaningful.

The D_2^+ ions were created by electron impact in a discharge ion source from D_2 gas, electrostatically accelerated to 40 keV at ion source platform 2, and injected into the CSR, where they were stored for up to 15 s. After ion injection, the CSR transfer beam line was switched to ion source platform 1, in order to prepare a neutral atomic carbon beam.

The initial C^- ions were produced in a sputter ion source, accelerated to either 118 or 122 keV and guided through the transfer beam line toward the CSR. A fraction of ∼2.4% of the ions were neutralized by the photodetachment laser, which was operated at 1.8 kW power (during laser-on phases), and switched on and off with a period of 30 ms. The neutral C atoms produced by photodetachment entered the ion-neutral interaction section of the CSR, while the remaining negative C^- beam was deflected upward, and collected in a dedicated Faraday cup behind the photodetachment section (see Fig. 3).

All deflectors and the energy analyzers in the CSR extraction beam line were set to the calibrated values to detect CD^+ product ions. The relative collision energy was varied by scanning the drift tube voltage in the photodetachment section (Fig. 4). All voltages relevant for the product guidance, like, e.g., the energy analyzers in the extraction section, were scaled with the expected total product energy during scans. As in previous studies[17], the kinetic energy release following Reaction 3 was ignored. We believe this to be a very good approximation, as we are working with rather high beam energies.

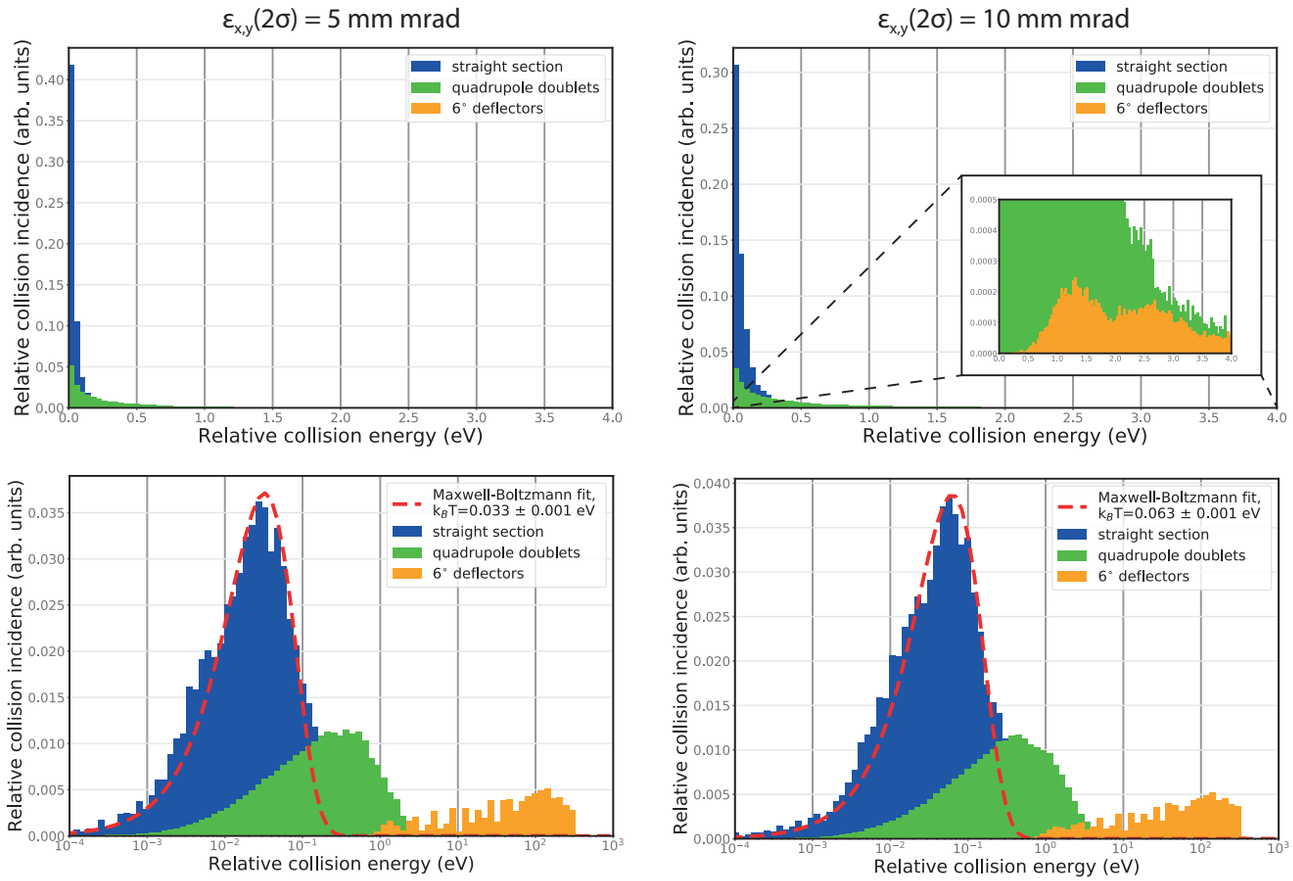

FIG. 11. The two panels on the left-hand side show the simulated collision energy histogram of two velocity-matched beams, namely a neutral C beam at 120 keV and a stored D_2^+ ion beam at a beam emittance of $\varepsilon_{x,y}(2\sigma) = 5$ mm mrad. The panels on the right-hand side depict a stored ion beam with an emittance of $\varepsilon_{x,y}(2\sigma) = 10$ mm mrad. The upper panels use a linear scale that affords a fair representation of the fraction of events occuring in the various sections of the interaction region at energies below 4 eV, while the lower panels use a logarithmic scale with increasing bin sizes to provide a better representation of the entire range of collision energies (this leads to a perceived overemphasis of the high collision energy part). The inset in the upper right panel is a magnification that shows the small fraction of events that takes place in the 6° deflectors and results in collision energies in the relevant range below 4 eV, before the strong drop of the rate cofficient at higher energies.

A. Merged beams rate coefficient

While we are not aiming at an independent and absolute rate coefficient measurement at this stage, we will describe the reaction rate coefficient and all relevant parameters for comparison to previous studies, and for future reference.

We can express the merged beams rate coefficient as a product of the energy-dependent cross section σ for Reaction 3 and the distribution of relative velocities v_r by[15,36]

$$\langle \sigma v_r \rangle = \frac{S}{T_P \eta} \frac{e^2}{I_C I_{D_2^+}} \frac{v_C v_{D_2^+}}{L\langle \Omega(z) \rangle}, \tag{7}$$

where S denotes the product (CD^+) count rate, T_P stands for the combined product transmission of the extraction beam line and the energy analyzers, e denotes the unit charge, η denotes the detection efficiency of the channeltron detector, I_C and $I_{D_2^+}$, stand for the currents of C atoms and D_2^+ ions, respectively, v_C and $v_{D_2^+}$ denote the velocities of the respective species, and $L\langle \Omega(z) \rangle$ stands for the product of the length of the interaction section L and the averaged overlap form factor.

The product signal S was derived from the count rate recorded in the channeltron detector behind the energy analyzers (Fig.9) during the laser-on phases, which was corrected for background events (see next section).

The transmission T_P of the energy analyzers for the product ions was estimated from our simulations and benchmark measurements with a continuous beam to be of the order of 90 ± 10 %. Furthermore, we assume a detection efficiency of $\eta = 95 \pm 5$ % for the channeltron detector at these energies.

The flux of C atoms I_C was recorded continuously using secondary electron emission in the neutral cup at the end of the extraction section (Fig. 5), and corrected by the secondary electron yield per neutral impact, denoted by γ. The value for γ was determined for each extended data taking run by dividing the average current recorded in the neutral cup during laser-on phases by the loss of the C^- ion current measured simultaneously in the ion beam dump upstream of the CSR in-

jection section (Fig. 6). Note that in line with previous merged beams studies[36], we express the neutral flux as a current I_C in amperes, artificially attributing a single charge to each neutral atom.

The ion current $I_{D_2^+}$ inside the CSR was determined in a two-step procedure. During the measurements we recorded the count rate R_N of a movable single-particle detector[41,42] situated in another section of the CSR. This detector was moved into a position where it captures the majority of particles neutralized by the residual gas in this section. The signal recorded here is assumed to be proportional to the number of ions stored inside the storage ring. To calibrate the signal on a absolute scale, we established a procedure where we bunch the ion beam – using a suitable radiofrequency signal – and measure the total current of the stored particles by the mirror charge induced in a calibrated current pickup electrode[26], while counting R_N at the same time. This procedure effectively allows us to infer the particle current $I_{D_2^+}$ during storage from the recorded neutralization count rate R_N. Since the proportionality depends on the storage ring vacuum, the calibration procedure is usually repeated daily in a data-taking campaign. We find that the pressure in the ring is usually stable to within 10% during a day of measurements. Larger fluctuations can sometimes be caused by rare temporal instabilities of the cryogenic helium supply, but they are apparent by a sudden change in the neutral count rate R_N in the data, and the affected injections can be discarded.

The velocities v_C and $v_{D_2^+}$ of the individual beams can be calculated from the beam energies, the overlap length L and form factor $\Omega(z)$ are taken from our simulations (see Sect. IV).

The overlap factor constitutes by far the largest uncertainty for our proof-of-principle measurement. Owing to problems with cryogenic amplifiers during initial runs with the neutral-beam setup, we were not able to confirm the exact positioning of the ion beam inside the CSR, introducing a large uncertainty for the beam overlap (the amplifiers have in the meantime been replaced with more reliable versions that can operate at room temperature). We will therefore refrain from giving an absolute rate coefficient for the present measurements and scale our results to previous measurements. Note that once the absolute scale has been calibrated, it would still be possible to perform meaningful measurements with different species under these conditions, as one of the advantage of electrostatic storage is that the ion beam trajectories are very reproducible and do not change for particle beams with different masses. We intend to make use of this fact for the absolute calibration of future measurement campaigns.

B. Background subtraction

The product count rate S of CD^+ ions resulting from Reaction 3 is derived from the count rate R_{on} measured in the channeltron detector during the laser-on phases of the experiment. The photodetachment laser is switched with a period of 30 ms and the count rate R_{off} during the laser-off phases is also recorded. During the laser-off phases there is a small but measurable neutral flux arriving at the neutral cup. These neutrals are created by electron stripping due to collisions of the C^- beam with the residual gas upstream of the C^- beam dump in the injection beam line. Since these neutrals result from gas stripping, they are not necessarily in the atomic ground state, on the contrary, they can occupy highly excited Rydberg states, which may have increased cross sections to react with the stored D_2^+ ions. To eliminate this type of background, we routinely subtract the count rate during the laser-off phases from the signal during laser-on phases.

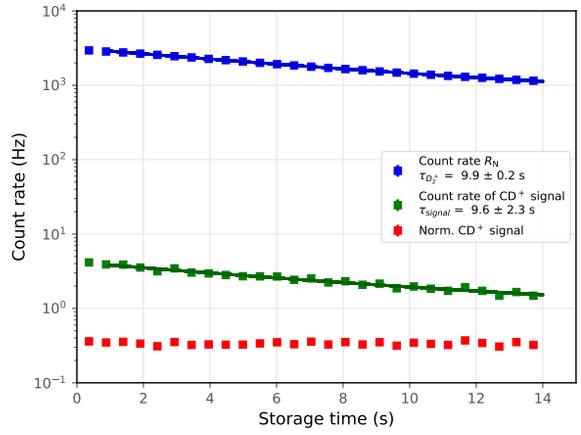

FIG. 12. The decay of the neutral count rate R_N, recorded by a single-particle detector in the electron cooler section, is shown by a blue line. This signal is proportional to the number of stored D_2^+ ions (see main text for details). The decay of the unnormalized CD^+ signal is shown by a green line. The respective lifetimes of a single exponential fit are given in the inset. The normalized CD^+ product signal is shown in red and found to be independent of the storage time. Statistical error bars, derived from counting statistics, are smaller than the size of the symbols, as the count rates are integrated across all relative energies.

Another form of background in the present experiment stems from C^+ ions that are created via electron stripping of the neutral C beam colliding with the residual gas in the region where the beam exits the CSR and enters the extraction beam line (inside and ahead the 15° deflector). However, this type of background is suppressed very efficiently by the double energy analyzers in front of the channeltron. Furthermore, we routinely remove all ions from the storage ring for a few seconds at the end of each injection cycle, while the laser sequence and the data taking continue. During these intervals we record the background counts R_{on}^0 created by the neutral beam alone, which we can average and subtract from the signal count rate. This procedure also allows us to discriminate potential background created by the stored D_2^+ beam, although we have not seen any evidence of background events caused by the stored ion beam.

The background-corrected count rate S used for our experimental results is given as

$$S = R_{on} - R_{off} - R_{on}^0 , \qquad (8)$$

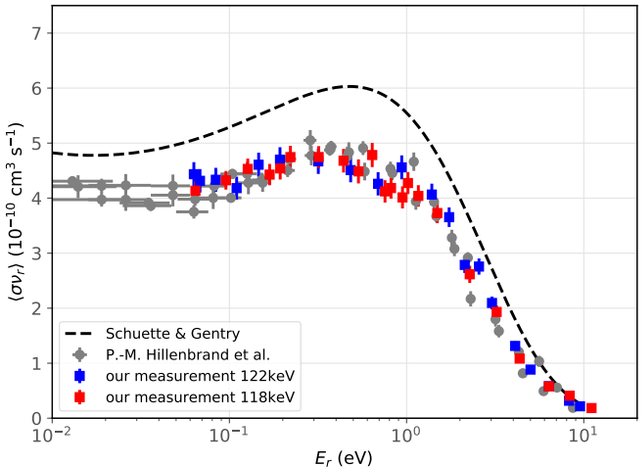

FIG. 13. Merged beams rate coefficient for the reaction C + $D_2^+ \rightarrow CD^+ + D$, measured at the CSR. The red and blue dots were obtained with initial C- beam energies of 122 and 118 keV, respectively, and the voltage-adjustable drift tube in the photodetachment section was used to tune the final neutral beam energy. The absolute scale was adapted to the previous results of Hillenbrand et al.[46] (grey dots). A fit to the previous experimental results of Schuette and Gentry[14] is shown by the dashed line.

where the event rate $R^0_{\rm on}$ recorded without ions in the ring is adjusted for the length of the measurement intervals.

C. Results

For the present proof-of-principle measurements we injected a large number of ions into the ring to facilitate the detection of the CD^+ signal. This usually leads to a fast initial decay component in the first seconds of storage. This fast decay is in all likelihood induced by space charge or intrabeam scattering effects, which depend on particle number and density of the stored beam. In this context, Fig. 12 serves as a cross check for our calibration and data acquisition routine. Shown is the decay of the neutral count rate R_N (blue line) recorded at the single-particle detector in the electron cooler section, which we use as a calibrated proxy of the number of stored ions. Also shown in the same plot is the CD^+ product signal S (green line), recorded in the channeltron detector at the end of the CSR extraction section, averaged over all collision energies. Since there will be no internal cooling of the D_2^+ beam during storage, we expect both decays to show a parallel trend, and we indeed find that both data sets can be modeled well with a single exponential decay with identical decay constants (within the uncertainties). Moreover, we find the normalized CD^+ signal (red curve) to be independent of the storage time, confirming that the merged beams overlap and the product transmission through the energy analyzers do not change during the critical phase of the first seconds of storage.

Our measured merged beams rate coefficient is plotted in Fig. 13 as a function of the relative collision energy. We plotted two curves, representing a scan during which we increased the initial energy of the C^- beam from 118 to 122 keV and a scan during which we decreased the beam energy from 122 keV to 118 keV. The energy of the stored D_2^+ ions was 40 keV in both cases. The good agreement between both data set serves as another cross-check for the validity of our beam simulation and data analysis procedures. The error bars for our data are purely statistical, they are derived from the accumulated counts in each bin, assuming Poisson statistics.

Also shown are the results of two previous measurements for comparison. An initial merged beams study of this reaction was carried out in 1982 by Schuette and Gentry[14]. In their measurement they used an electron impact ion source for the D_2^+ beam, while the atomic C beam was created by charge exchange of C^+ in a vapor cell. This procedure may result in the creation of excited C atoms, although the authors argue that they expect to produce primarily atoms in the C(^3P) ground term by charge exchange with xenon gas[14].

Very recently, single pass merged beams measurements were carried out for collisions between C atoms and both H_2^+ and D_2^+ ions[46] by Hillenbrand et al. In this case the neutral C atoms were produced by laser photodetachment, in a setup very similar to the one used for the present work, yielding only C atoms in the ^3P ground term. Their measured rate coefficient for the C + D_2^+ reaction is essentially compatible with the previous experiment of Schuette and Gentry across all collision energies, but on average it is about 20% lower. We consider the more recent data of Hillenbrand et al. to be more reliable, in particular due to the possible contamination of the neutral beam with excited C atoms in the previous study[14]. Consequently the absolute scale of our measurements was scaled to the more modern experiment of Hillenbrand et al.[46]

While for our experiment, as well as the study of Hillenbrand et al., all neutral atoms will occupy the ^3P ground term, there is no control over the distribution of the $J = 0, 1, 2$ fine structure levels, which we assume to be thermal. Regardless of the validity of this assumption, our setup for the anion beam and the neutralization scheme are essentially the same as in the study of Hillenbrand et al., and therefore we do not expect significant differences in the fine structure populations among these two experiments.

Likewise, we expect the internal excitation of our D_2^+ ions to be similar to both previous experiments, assuming that electron impact in our discharge ion source will lead to an essentially vertical transition from D_2 ($X^1\Sigma_g^+$) to D_2^+ ($X^2\Sigma_g^+$)[47]. Implicitly, this also presumes that there are no ion-neutral collisions taking place inside the ions source that could potentially alter the internal excitation after the ionization process. This is probably a good approximation, as the ion source was operated with pure D_2 gas, and collisions of D_2^+ with D_2 should predominantly lead to the strongly exothermic formation of triatomic deuterium ions D_3^+, rather than inelastic change of internal energy.

The overall energy-dependence of our measured merged beams rate coefficient is in very good agreement with both previous studies. We have assumed a resolution limit of

$\sim$60 meV for the present study, corresponding to a typical emittance value of $\varepsilon_{x,y}(2\sigma)\sim$10 mm mrad.

The overall agreement between our results and both previous measurements is very encouraging. We are currently working on improved diagnostic means including imaging to establish the beam overlap better. Moreover, first attempts to work with electron-cooled ion beams are underway.

VI. SUMMARY AND OUTLOOK

We have constructed a dedicated setup to study ion-neutral collisions at the heavy ion storage ring CSR, to the best of our knowledge the first of its kind. The neutrals are created by photodetachment of negative ions, resulting in a fast beam of pure ground term atoms. The neutral beam energy can be varied in a voltage-adjustable drift tube. The neutral beam is superimposed to the stored molecular ions in one of the straight sections of the CSR. Our experiment allows for the detection of charged products resulting from collisions between ground term atoms and stored molecular ions. Furthermore, the merged beams configuration enables energy-resolved measurements over a wide range of collision energies.

Our simulations show that the main factor influencing the energy resolution of the experiment is the emittance of the stored ion beam. While the present experiment has a moderate resolution around 60 meV, our understanding of the electrostatic storage ring dynamics keeps improving, and we have recently achieved lower beam emittance values by better matching the injected beam Twiss parameters to the CSR machine parameters. To define the overlap between both beams better, we have recently performed extensive studies using imaging in the electron cooler section. As our understanding of the storage ring optical lattice increases, it becomes possible to use the imaging data – in combination with detailed simulations of the beam dynamics – to predict the shape of the beam in the overlap section of the neutral beam setup. We are also considering to introduce wire scanners into this section to verify our simulations. The most straightforward approach, however, may be to apply electron cooling to decrease the ion beam diameter. Once the ion beam is substantially smaller than the neutral beam, its shape has only a minor influence on the overlap factor, as the neutral beam is rather homogeneous. The same principle applies for merged beams measurements of electron-ion collisions at storage rings, where it allows for accurate and reproducible measurements of rate coefficients on an absolute scale. The application of electron cooling for improved beam quality in combination with the neutral beam experiment is currently being pursued.

While for the present measurements the C + D_2^+ collision system was chosen specifically to reproduce previous single-pass experiments, the implementation of an ion-atom merged beams setup at a cryogenic storage ring opens up unique opportunities for future measurements. As a first step, collisions involving infrared-active ions like, e.g., HD^+, H_2D^+, HeH^+, CH^+ and numerous other species of astrophysical interest can be studied, making use of the fact that these molecules will cool to their lowest quantum states during storage[29,33]. This will yield data that are much more adequate for use in astrophysical models compared to single-pass experiments, which sample molecular ions with unknown rotational and vibrational excitation. In fact, data on collisions of C atoms with HD^+ and H_2D^+ have recently been taken at the CSR, and initial studies on the important primordial reaction of HeH^+ with D have been carried out. Furthermore, the fact that the CSR can be operated with pulsed ion sources is another significant advantage, compared to single-pass setups. For example, the probably most important species of astrophysical interest is the triatomic hydrogen ion H_3^+. While the production of H_3^+ in standard ion sources leads to extremely high internal excitation[48], it can be pre-cooled in cryogenic ion traps or supersonic expansion sources in pulsed operation[4,25]. Diagnostic efforts to determine the population of individual rotational states inside the storage ring by laser diagnostic schemes are currently being developed[49]. In combination, these techniques and the setup presented here pave the way for experiments on some of the most frequent and important molecular reactions in the universe, under true interstellar conditions.

In summary, we present the first measurements for reactive ion-neutral merged beams measurements obtained at a heavy-ion storage ring. The energy-dependence of our results agrees well with previous studies. Data on collisions of C atoms with HD^+ and H_2D^+ molecules, which both possess a dipole moment and thus cool during storage inside the CSR, are currently being analyzed. Efforts to improve the definition of the ion beam emittance and the beam overlaps are underway and will be reported in due time.

ACKNOWLEDGMENTS

This work was supported by the Max Planck Society. F.G., A.P.O., and H.K. were supported by the European Research Council under Grant Agreement No. StG 307163. X.U. is a Senior Research Associate of the Fonds de la Recherche Scientifique - FNRS, and acknowledges support under grant no. 4.4504.10. We thank Charles C. Havener for valuable advice and fruitful discussions.

[1] X. Urbain, A. Cornet, F. Brouillard, and A. Giusti-Suzor, Phys. Rev. Lett. **66**, 1685 (1991).
[2] F. Brouillard and X. Urbain, Physica Scripta **2002**, 86 (2002).
[3] P. C. Stancil, C. C. Havener, P. S. Krstić, D. R. Schultz, M. Kimura, J. P. Gu, G. Hirsch, R. J. Buenker, and B. Zygelman, Astrophys. J. **502**, 1006 (1998).
[4] H. Kreckel, H. Bruhns, M. Čížek, S. C. O. Glover, K. A. Miller, X. Urbain, and D. W. Savin, Science **329**, 69 (2010).
[5] C. C. Havener, M. S. Huq, H. F. Krause, P. A. Schulz, and R. A. Phaneuf, Phys. Rev. A **39**, 1725 (1989).
[6] C. C. Havener, M. P. Nesnidal, M. R. Porter, and R. A. Phaneuf, Nucl. Instrum. Methods Phys. Res. B **56**, 95 (1991).
[7] H. Bruhns, H. Kreckel, D. W. Savin, D. G. Seely, and C. C. Havener, Phys. Rev. A **77**, 064702 (2008).
[8] I. N. Draganić, D. G. Seely, and C. C. Havener, Phys. Rev. A **83**, 054701 (2011).

[9]W. Schön, S. Krüdener, F. Melchert, K. Rinn, M. Wagner, E. Salzborn, M. Karemera, S. Szücs, M. Terao, D. Fussen, R. Janev, X. Urbain, and F. Brouillard, Phys. Rev. Lett. **59**, 1565 (1987).
[10]A. Le Padellec, T. Launoy, A. Dochain, and X. Urbain, J. Phys. B: At. Mol. Opt. Phys. **50**, 095202 (2017).
[11]N. de Ruette, A. Dochain, T. Launoy, R. F. Nascimento, M. Kaminska, M. H. Stockett, N. Vaeck, H. T. Schmidt, H. Cederquist, and X. Urbain, Phys. Rev. Lett. **121**, 083401 (2018).
[12]T. Launoy, J. Loreau, A. Dochain, J. Liévin, N. Vaeck, and X. Urbain, Astrophys. J. **883**, 85 (2019).
[13]W. R. Gentry, D. J. McClure, and C. H. Douglass, Rev. Sci. Instrum. **46**, 367 (1975).
[14]G. F. Schuette and W. R. Gentry, J. Chem. Phys. **78**, 1777 (1983).
[15]A. P. O'Connor, X. Urbain, J. Stützel, K. A. Miller, N. de Ruette, M. Garrido, and D. W. Savin, Astrophs. J. Suppl. **219**, 6 (2015).
[16]N. de Ruette, K. A. Miller, A. P. O'Connor, X. Urbain, C. F. Buzard, S. Vissapragada, and D. W. Savin, Astrophys. J. **816**, 31 (2016).
[17]P. M. Hillenbrand, K. P. Bowen, J. Liévin, X. Urbain, and D. W. Savin, Astrophys. J. **877**, 38 (2019).
[18]A. B. Henson, S. Gersten, Y. Shagam, J. Narevicius, and E. Narevicius, Science **338**, 234 (2012).
[19]A. Osterwalder, EPJ Techn. Instrum. **2**, 10 (2015).
[20]S. M. Trujillo, R. H. Neynaber, L. Marino, and E. W. Rothe, *Proc. of the IVth Int. Conf. on the Physics of Electronic and Atomic Collisions* (Science Bookcrafters, 1965) p. 260.
[21]A. Auerbach, R. Cacak, T. D. Gaily, C. J. Keyser, J. B. A. Mitchell, S. F. J. Wilk, R. Caudano, and J. W. McGowan, J. Phys. B: At. Mol. Opt. Phys. **10**, 3797 (1977).
[22]S. Schippers, Nucl. Instrum. Methods Phys. Res. B **350**, 61 (2015).
[23]M. Larsson and A. E. Orel, *Dissociative Recombination of Molecular Ions*, Cambridge Molecular Science (Cambridge University Press, 2008).
[24]A. Al-Khalili, S. Rosén, H. Danared, A. M. Derkatch, A. Källberg, M. Larsson, A. Le Padellec, A. Neau, J. Semaniak, R. Thomas, M. Af Ugglas, L. Vikor, W. Zong, W. J. van der Zand e, X. Urbain, M. J. Jensen, R. C. Bilodeau, O. Heber, H. B. Pedersen, C. P. Safvan, L. H. Andersen, M. Lange, J. Levin, G. Gwinner, L. Knoll, M. Scheffel, D. Schwalm, R. Wester, D. Zajfman, and A. Wolf, Phys. Rev. A **68**, 042702 (2003).
[25]H. Kreckel, M. Motsch, J. Mikosch, J. Glosík, R. Plašil, S. Altevogt, V. Andrianarijaona, H. Buhr, J. Hoffmann, L. Lammich, M. Lestinsky, I. Nevo, S. Novotny, D. A. Orlov, H. B. Pedersen, F. Sprenger, A. S. Terekhov, J. Toker, R. Wester, D. Gerlich, D. Schwalm, A. Wolf, and D. Zajfman, Phys. Rev. Lett. **95**, 263201 (2005).
[26]R. von Hahn, A. Becker, F. Berg, K. Blaum, C. Breitenfeldt, H. Fadil, F. Fellenberger, M. Froese, S. George, J. Göck, M. Grieser, F. Grussie, E. A. Guerin, O. Heber, P. Herwig, J. Karthein, C. Krantz, H. Kreckel, M. Lange, F. Laux, S. Lohmann, S. Menk, C. Meyer, P. M. Mishra, O. Novotný, A. P. O'Connor, D. A. Orlov, M. L. Rappaport, R. Repnow, S. Saurabh, S. Schippers, C. D. Schröter, D. Schwalm, L. Schweikhard, T. Sieber, A. Shornikov, K. Spruck, S. Sunil Kumar, J. Ullrich, X. Urbain, S. Vogel, P. Wilhelm, A. Wolf, and D. Zajfman, Rev. Sci. Instrum. **87**, 063115 (2016).
[27]Y. Nakano, Y. Enomoto, T. Masunaga, S. Menk, P. Bertier, and T. Azuma, Rev. Sci. Instrum. **88**, 033110 (2017).
[28]H. T. Schmidt, R. D. Thomas, M. Gatchell, S. Rosén, P. Reinhed, P. Löfgren, L. Brännholm, M. Blom, M. Björkhage, E. Bäckström, J. D. Alexander, S. Leontein, D. Hanstorp, H. Zettergren, L. Liljeby, A. Källberg, A. Simonsson, F. Hellberg, S. Mannervik, M. Larsson, W. D. Geppert, K. G. Rensfelt, H. Danared, A. Paál, M. Masuda, P. Halldén, G. Andler, M. H. Stockett, T. Chen, G. Källersjö, J. Weimer, K. Hansen, H. Hartman, and H. Cederquist, Rev. Sci. Instrum. **84**, 055115-055115-6 (2013).
[29]A. P. O'Connor, A. Becker, K. Blaum, C. Breitenfeldt, S. George, J. Göck, M. Grieser, F. Grussie, E. A. Guerin, R. von Hahn, U. Hechtfischer, P. Herwig, J. Karthein, C. Krantz, H. Kreckel, S. Lohmann, C. Meyer, P. M. Mishra, O. Novotný, R. Repnow, S. Saurabh, D. Schwalm, K. Spruck, S. Sunil Kumar, S. Vogel, and A. Wolf, Phys. Rev. Lett. **116**, 113002 (2016).
[30]C. Meyer, A. Becker, K. Blaum, C. Breitenfeldt, S. George, J. Göck, M. Grieser, F. Grussie, E. A. Guerin, R. von Hahn, P. Herwig, C. Krantz, H. Kreckel, J. Lion, S. Lohmann, P. M. Mishra, O. Novotný, A. P. O'Connor, R. Repnow, S. Saurabh, D. Schwalm, L. Schweikhard, K. Spruck, S. Sunil Kumar, S. Vogel, and A. Wolf, Phys. Rev. Lett. **119**, 023202 (2017).
[31]H. T. Schmidt, G. Eklund, K. C. Chartkunchand, E. K. Anderson, M. Kamińska, N. de Ruette, R. D. Thomas, M. K. Kristiansson, M. Gatchell, P. Reinhed, S. Rosén, A. Simonsson, A. Källberg, P. Löfgren, S. Mannervik, H. Zettergren, and H. Cederquist, Phys. Rev. Lett. **119**, 073001 (2017).
[32]H. T. Schmidt, G. Eklund, K. C. Chartkunchand, E. K. Anderson, M. Kamińska, N. de Ruette, R. D. Thomas, M. K. Kristiansson, M. Gatchell, P. Reinhed, S. Rosén, A. Simonsson, A. Källberg, P. Löfgren, S. Mannervik, H. Zettergren, and H. Cederquist, Phys. Rev. Lett. **121**, 079901 (2018).
[33]O. Novotný, P. Wilhelm, D. Paul, Á. Kálosi, S. Saurabh, A. Becker, K. Blaum, S. George, J. Göck, M. Grieser, F. Grussie, R. von Hahn, C. Krantz, H. Kreckel, C. Meyer, P. M. Mishra, D. Muell, F. Nuesslein, D. A. Orlov, M. Rimmler, V. C. Schmidt, A. Shornikov, A. S. Terekhov, S. Vogel, D. Zajfman, and A. Wolf, Science **365**, 676 (2019).
[34]R. A. Phaneuf, C. C. Havener, G. H. Dunn, and A. Müller, Rep. Prog. Phys. **62**, 1143 (1999).
[35]F. Grussie *et al.*, To be published.
[36]H. Bruhns, H. Kreckel, K. Miller, M. Lestinsky, B. Seredyuk, W. Mitthumsiri, B. L. Schmitt, M. Schnell, X. Urbain, M. L. Rappaport, C. C. Havener, and D. W. Savin, Rev. Sci. Instrum. **81**, 013112 (2010).
[37]A. P. O'Connor, F. Grussie, H. Bruhns, N. de Ruette, T. P. Koenning, K. A. Miller, D. W. Savin, J. Stuetzel, X. Urbain, and H. Kreckel, Rev. Sci. Instrum. **86**, 113306 (2015).
[38]F. Grussie, *Experimental studies of ion-neutral reactions under astrophysical conditions*, Ph.D. thesis, Heidelberg University (2016).
[39]J. A. Arnaud, W. M. Hubbard, G. D. Mandeville, B. de La Clavière, E. A. Franke, and J. M. Franke, Appl. Opt. **10**, 2775 (1971).
[40]H. R. Bilger and T. Habib, Appl. Opt. **24**, 686 (1985).
[41]K. Spruck, A. Becker, F. Fellenberger, M. Grieser, R. von Hahn, V. Klinkhamer, O. Novotnỳ, S. Schippers, S. Vogel, A. Wolf, *et al.*, Rev. Sci. Instrum. **86**, 023303 (2015).
[42]C. Krantz, O. Novotný, A. Becker, S. George, M. Grieser, R. von Hahn, C. Meyer, S. Schippers, K. Spruck, S. Vogel, and A. Wolf, Nucl. Instrum. Methods. Phys. Res. A **851**, 92 (2017).
[43]H. Grote and F. Schmidt, "MAD-X - An Upgrade from MAD8," `CERN-AB-2003-024ABP`.
[44]G4beamline, `http://g4beamline.muonsinc.com`.
[45]Copham Antenna System, Vectorfields Simulation Software, Kidlington, UK.
[46]P.-M. Hillenbrand, K. P. Bowen, F. Dayou, K. A. Miller, N. de Ruette, X. Urbain, and D. W. Savin, Phys. Chem. Chem. Phys. **22**, 27364 (2020).
[47]F. von Busch and G. H. Dunn, Phys. Rev. A **5**, 1726 (1972).
[48]H. Kreckel, S. Krohn, L. Lammich, M. Lange, J. Levin, M. Scheffel, D. Schwalm, J. Tennyson, Z. Vager, R. Wester, A. Wolf, and D. Zajfman, Phys. Rev. A **66**, 052509 (2002).
[49]A. Znotins, F. Grussie, A. Wolf, X. Urbain, and H. Kreckel, J. Mol. Spectr. **378**, 111476 (2021).

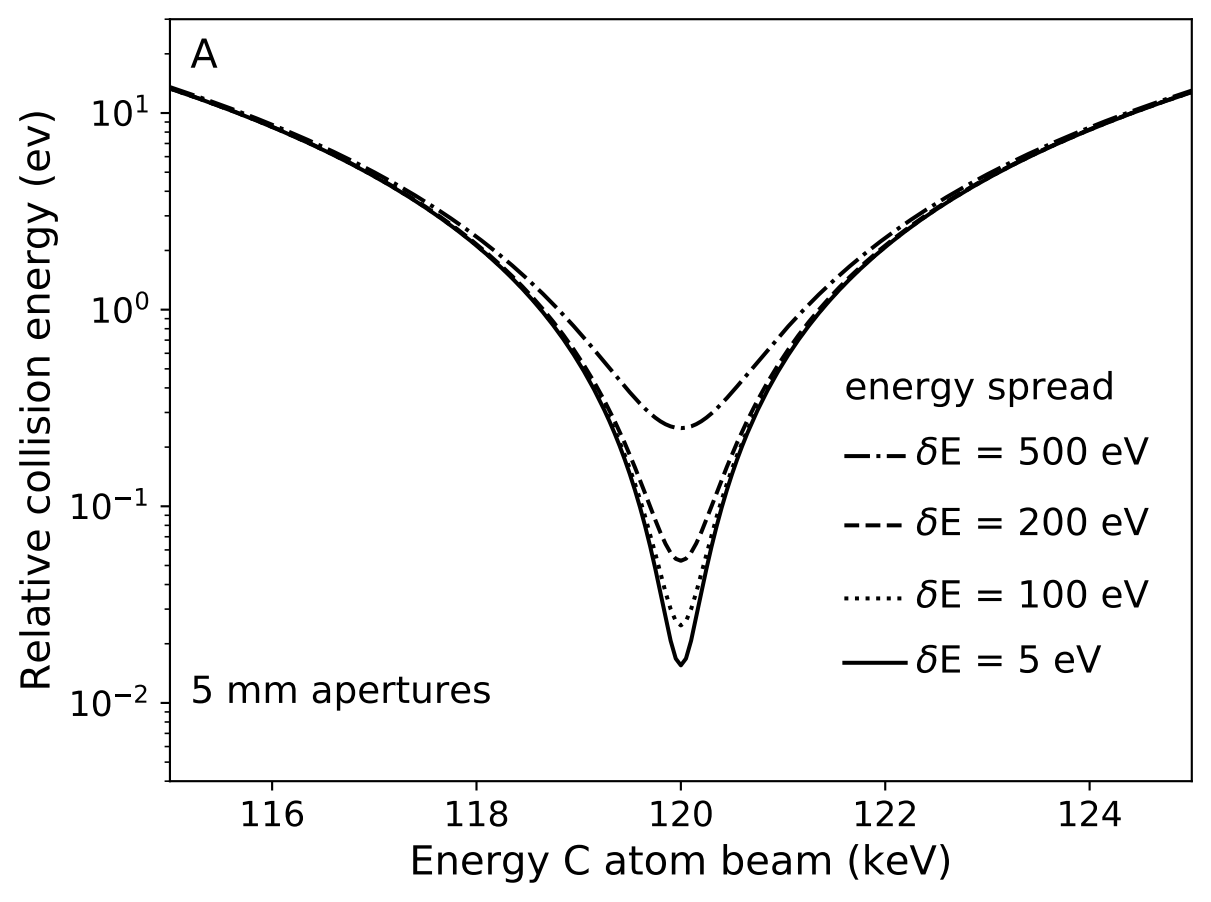
A
Relative collision energy (ev)
10^1
10^0
10^{-1}
10^{-2}
5 mm apertures
energy spread
δE = 500 eV
δE = 200 eV
δE = 100 eV
δE = 5 eV
116
118
120
122
124
Energy C atom beam (keV)

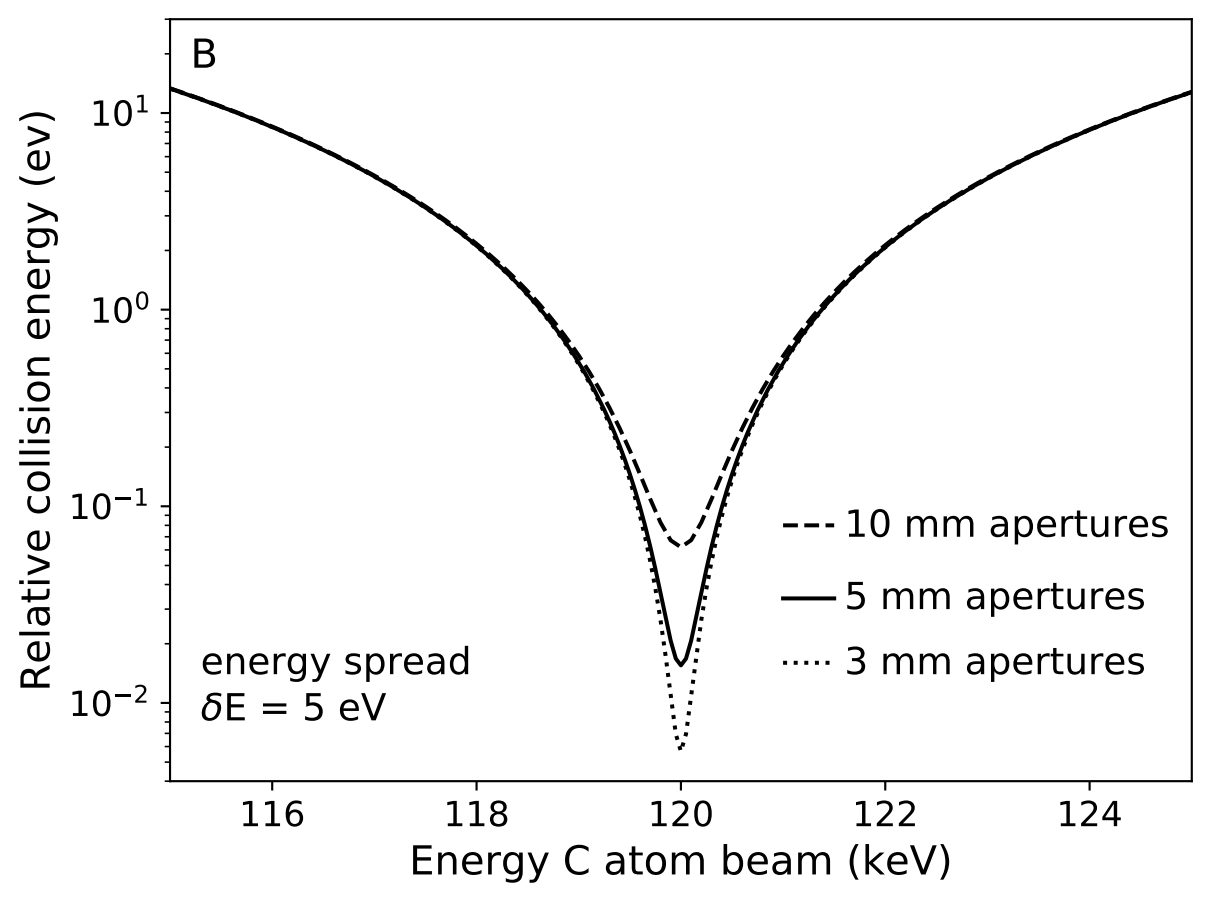
B
Relative collision energy (ev)
10^1
10^0
10^{-1}
10^{-2}
10 mm apertures
5 mm apertures
3 mm apertures
energy spread
δE = 5 eV
116
118
120
122
124
Energy C atom beam (keV)

Ion source

platform 2
(10-60 keV)

Mass selection

Cryogenic
Storage
Ring

Product
detector
(Channeltron)

Ion-neutral
interaction zone

Laser photodetachment

Mass selection

Switchable
beam
deflector

Movable
apertures

Neutral beam

Movable, cryogenic
product detectors

Extraction
beam line

10 m

Ion source platform 1 (10-300 keV)

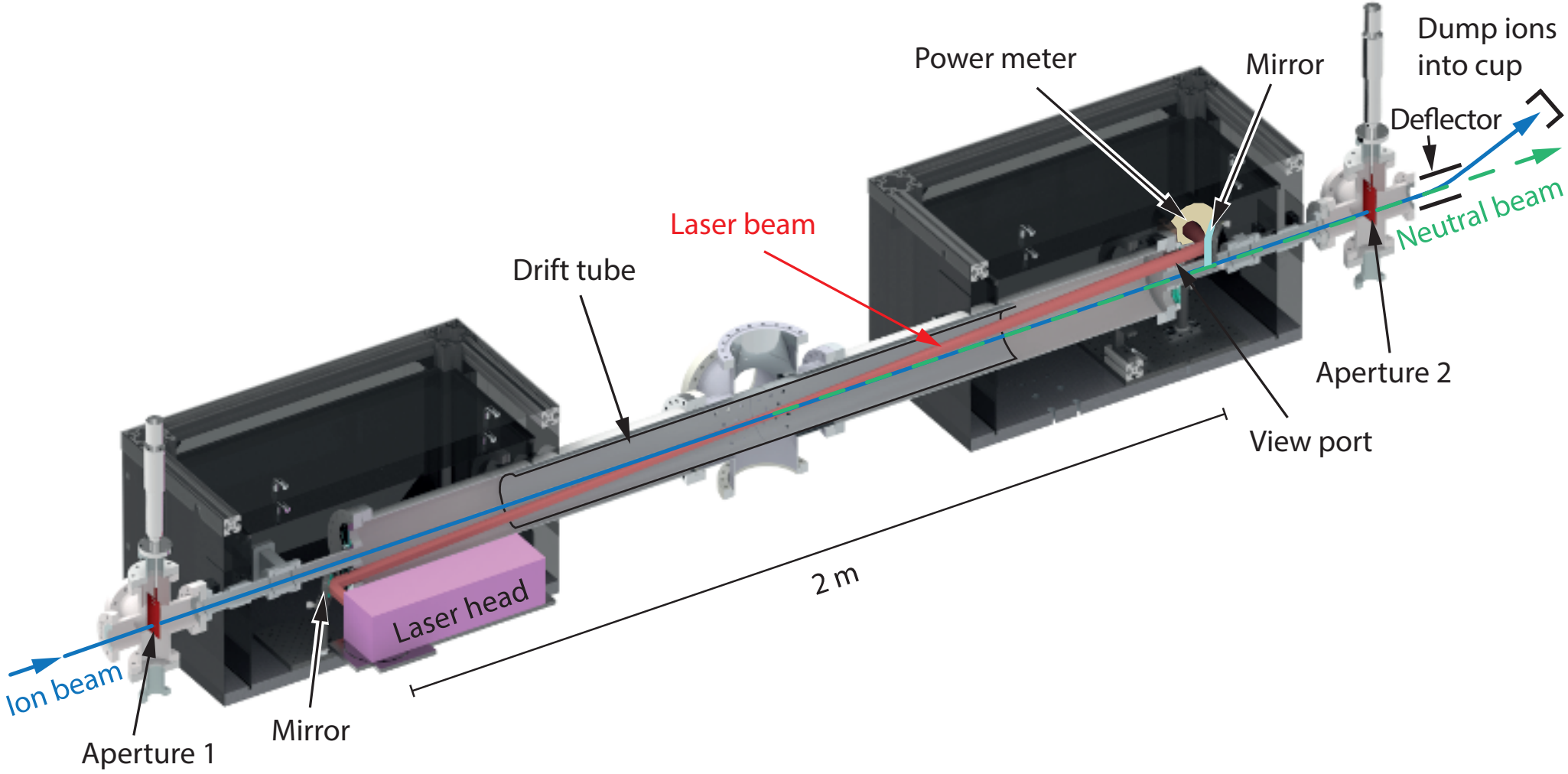
Power meter
Mirror
Dump ions into cup
Deflector
Laser beam
Drift tube
Neutral beam
Aperture 2
View port
2 m
Laser head
Ion beam
Aperture 1
Mirror

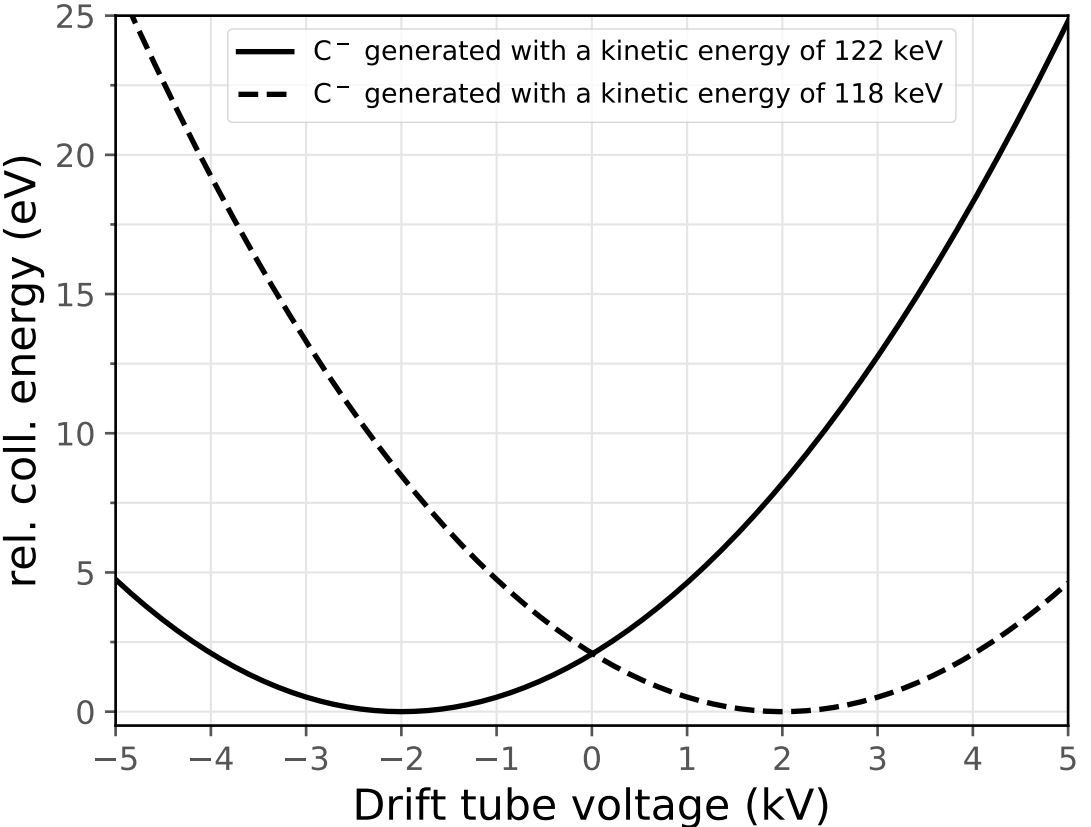
C⁻ generated with a kinetic energy of 122 keV
C⁻ generated with a kinetic energy of 118 keV
rel. coll. energy (eV)
Drift tube voltage (kV)
25
20
15
10
5
0
−5
−4
−3
−2
−1
0
1
2
3
4
5

Knife edge scanner (view in beam direction)

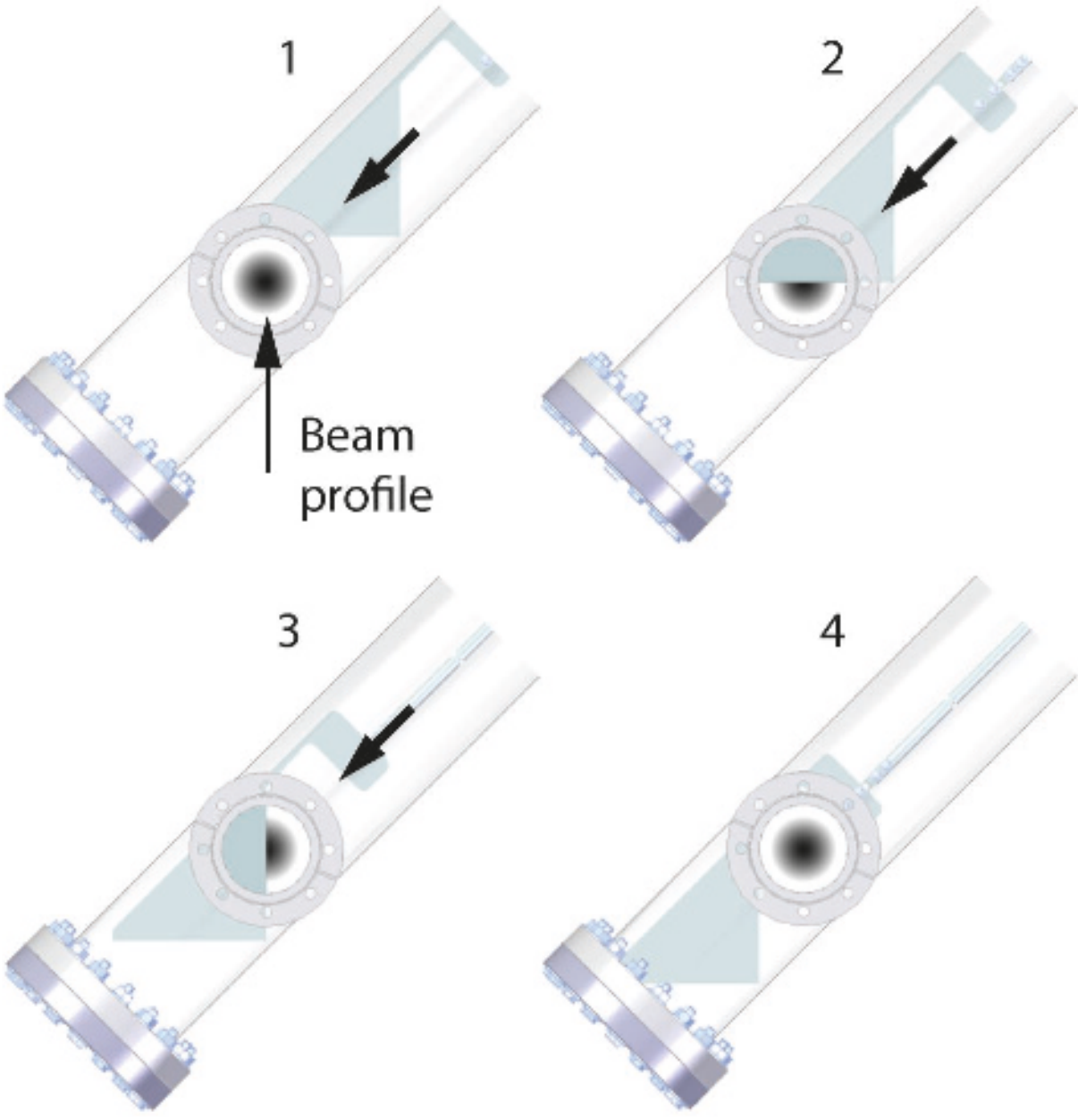

Neutral cup

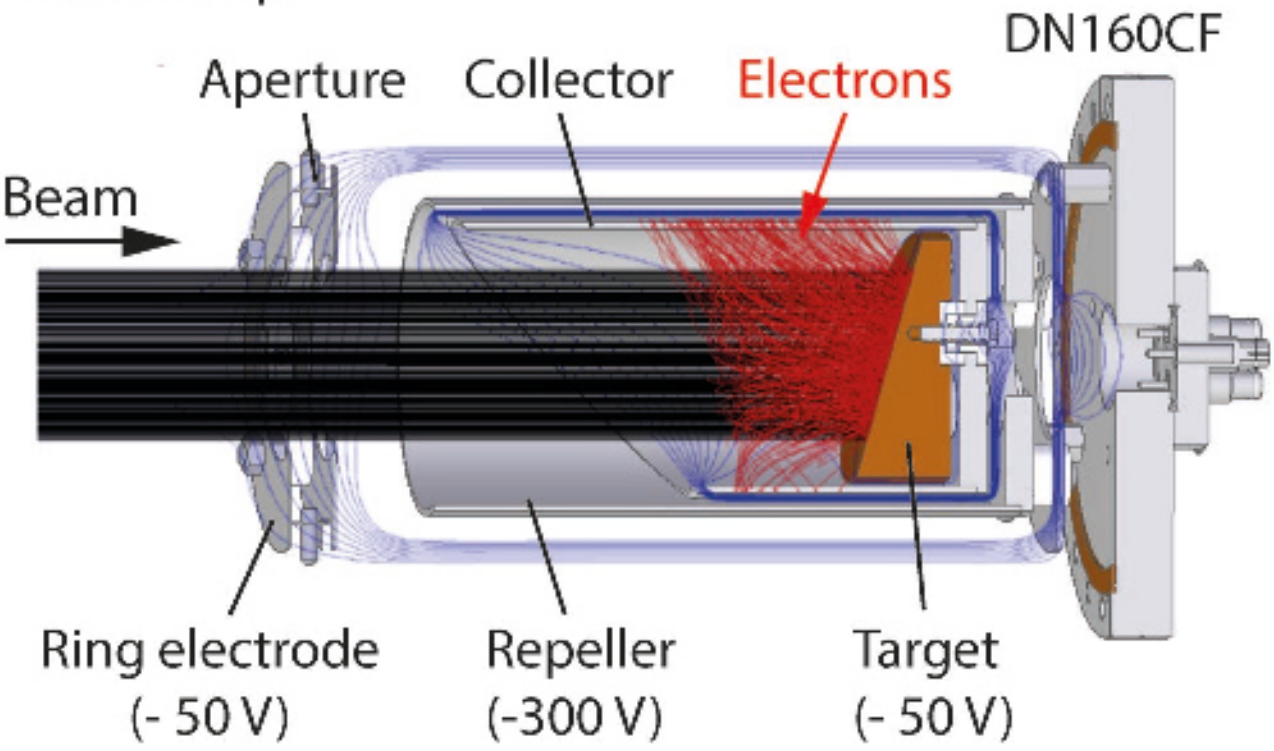

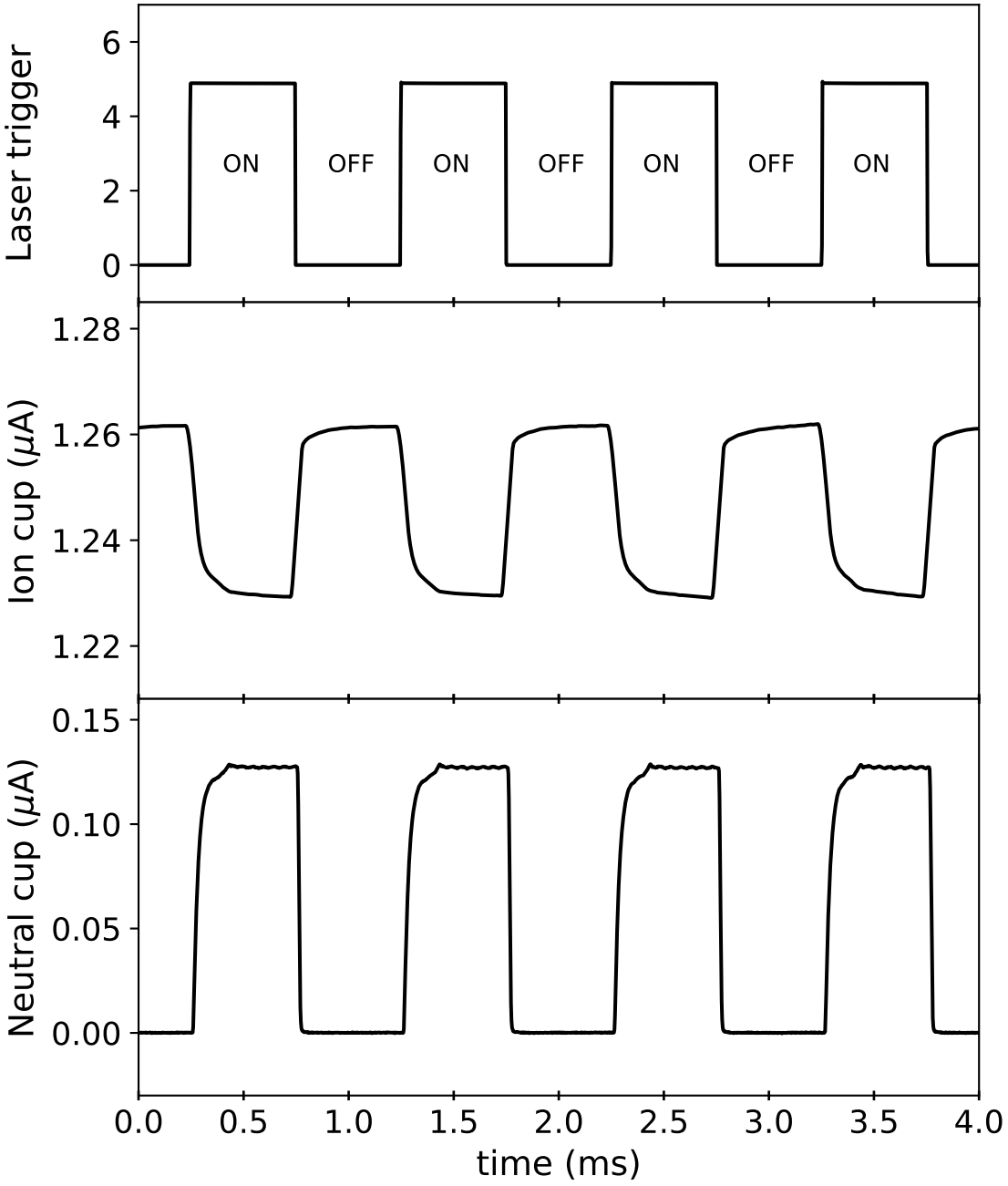
Laser trigger
6
4
2
0
ON
OFF
ON
OFF
ON
OFF
ON
Ion cup (μA)
1.28
1.26
1.24
1.22
Neutral cup (μA)
0.15
0.10
0.05
0.00
0.0
0.5
1.0
1.5
2.0
2.5
3.0
3.5
4.0
time (ms)

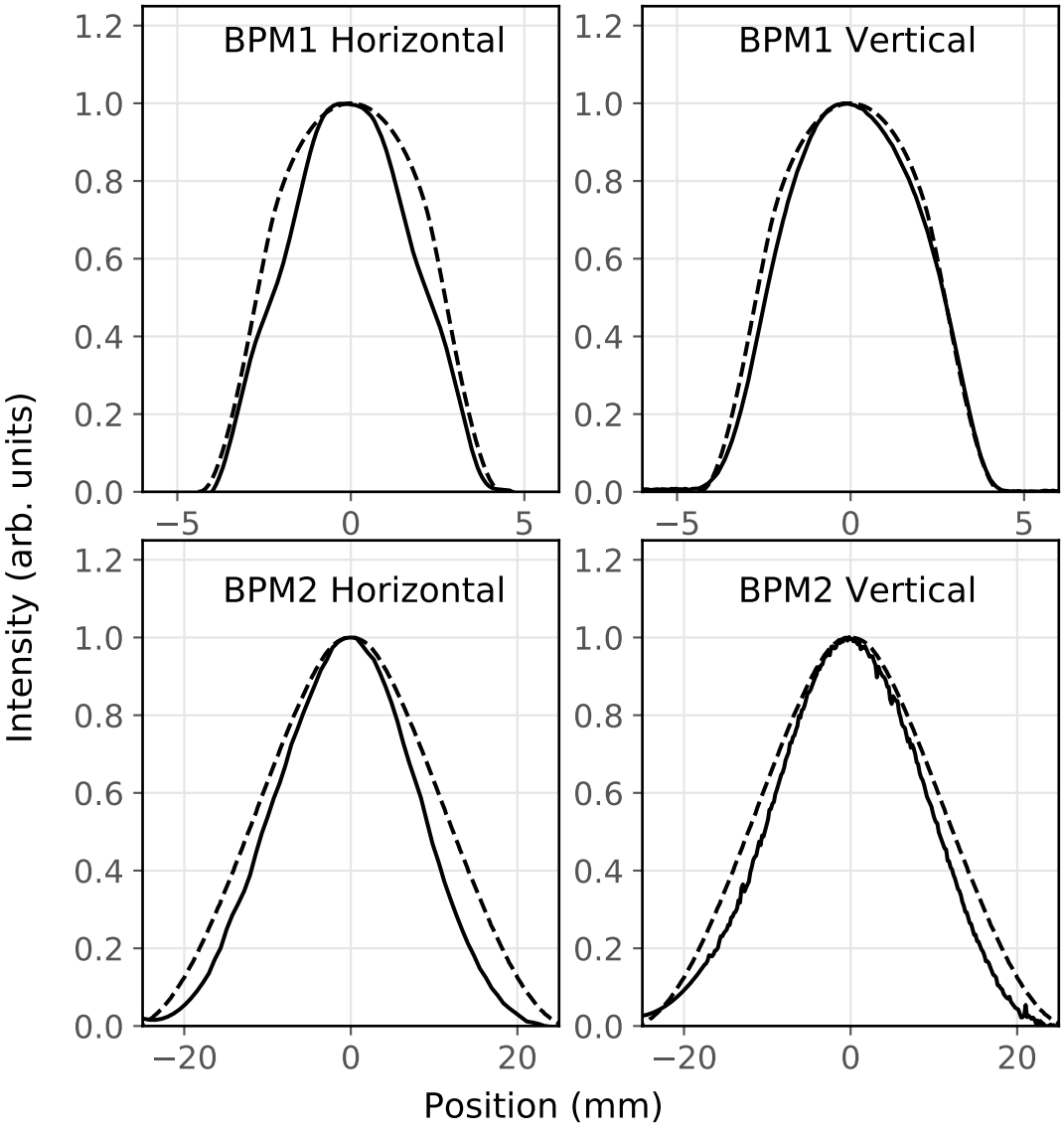
BPM1 Horizontal
BPM1 Vertical
BPM2 Horizontal
BPM2 Vertical
Intensity (arb. units)
Position (mm)
0.0
0.2
0.4
0.6
0.8
1.0
1.2
−5
0
5
−20
0
20

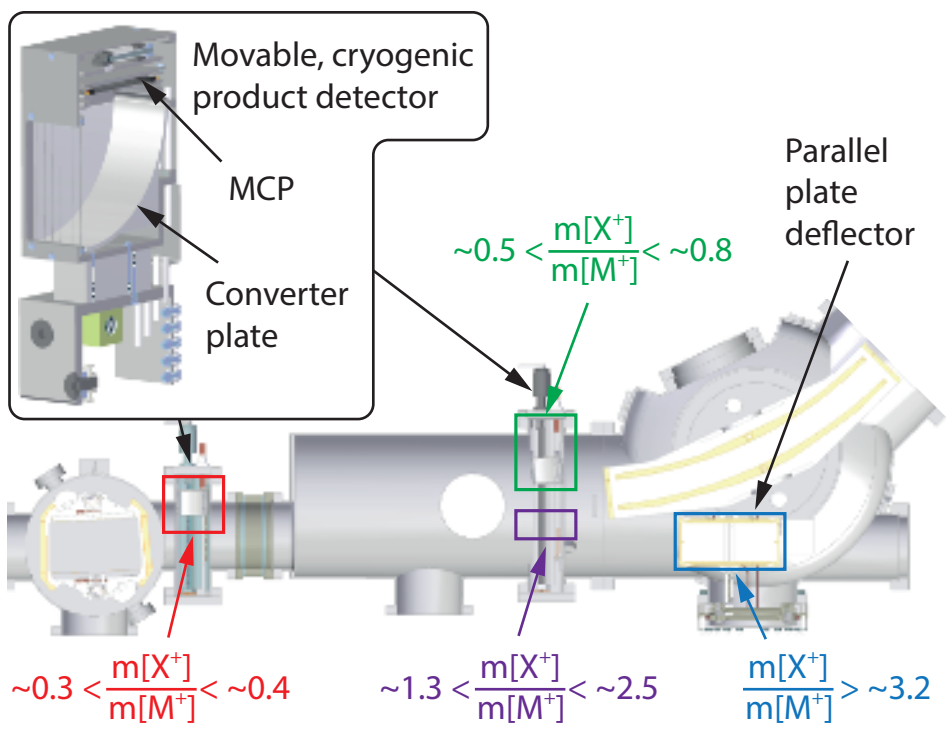
Movable, cryogenic product detector
MCP
Converter plate
Parallel plate deflector
~0.5 < m[X+]/m[M+] < ~0.8
~0.3 < m[X+]/m[M+] < ~0.4
~1.3 < m[X+]/m[M+] < ~2.5
m[X+]/m[M+] > ~3.2

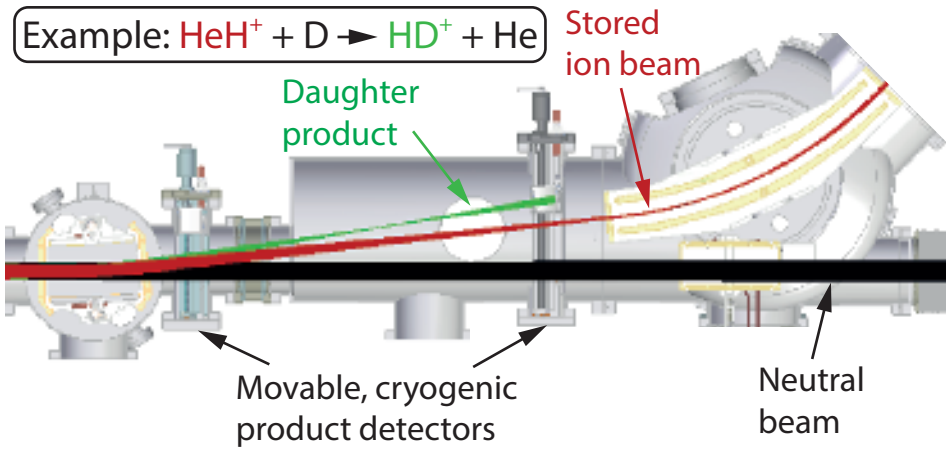
Example: HeH+ + D → HD+ + He
Stored ion beam
Daughter product
Movable, cryogenic product detectors
Neutral beam

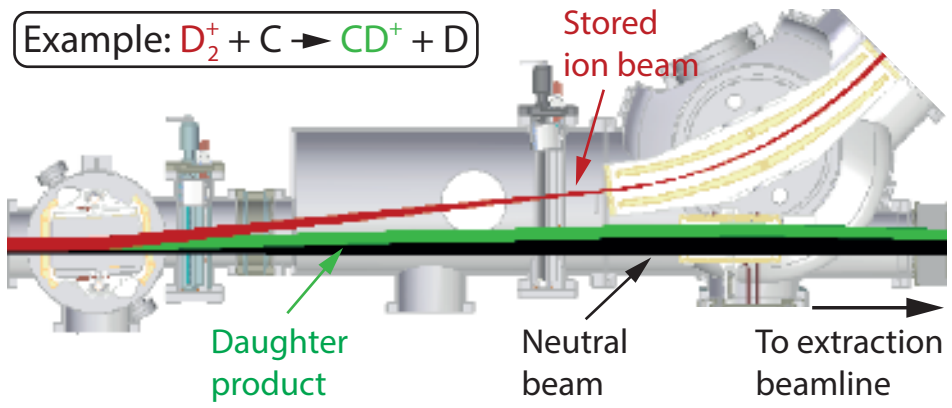
Example: D2+ + C → CD+ + D
Stored ion beam
Daughter product
Neutral beam
To extraction beamline

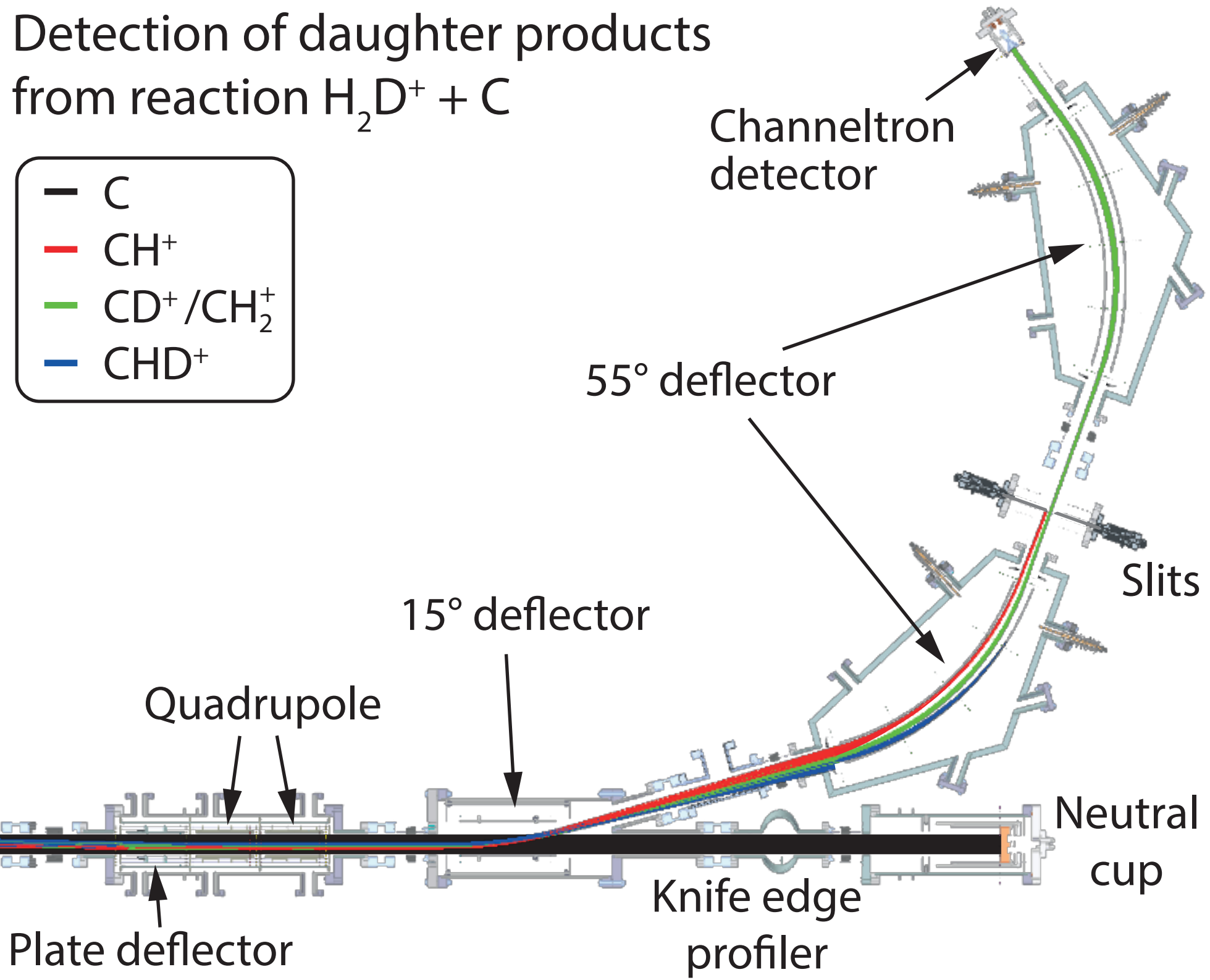
Detection of daughter products from reaction $H_2D^+ + C$
C
CH^+
CD^+ / CH_2^+
CHD^+
Channeltron detector
55° deflector
Slits
15° deflector
Quadrupole
Neutral cup
Knife edge profiler
Plate deflector

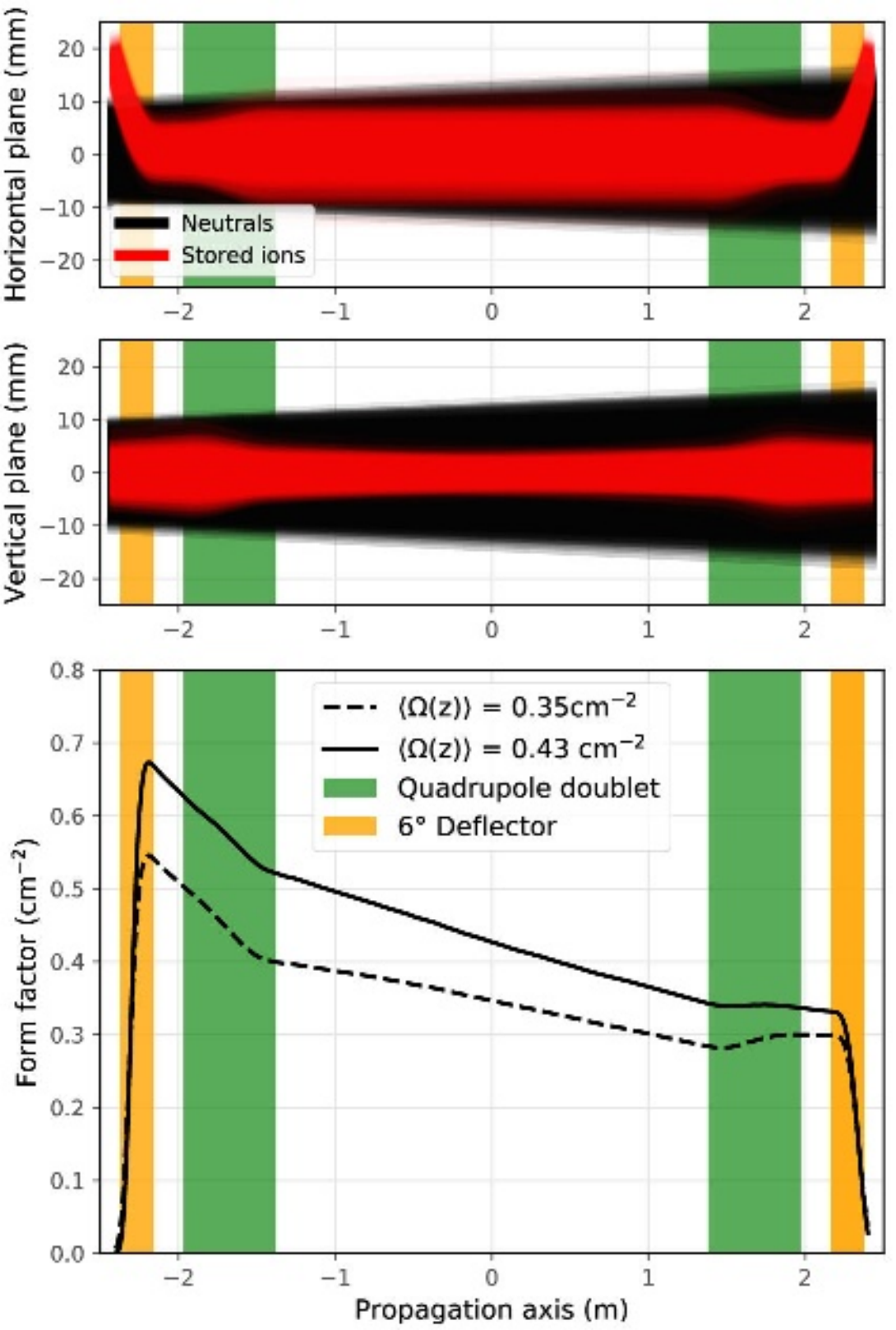
Horizontal plane (mm)
Neutrals
Stored ions
Vertical plane (mm)
Form factor (cm^{-2})
$\langle\Omega(z)\rangle$ = 0.35cm^{-2}
$\langle\Omega(z)\rangle$ = 0.43 cm^{-2}
Quadrupole doublet
6° Deflector
Propagation axis (m)

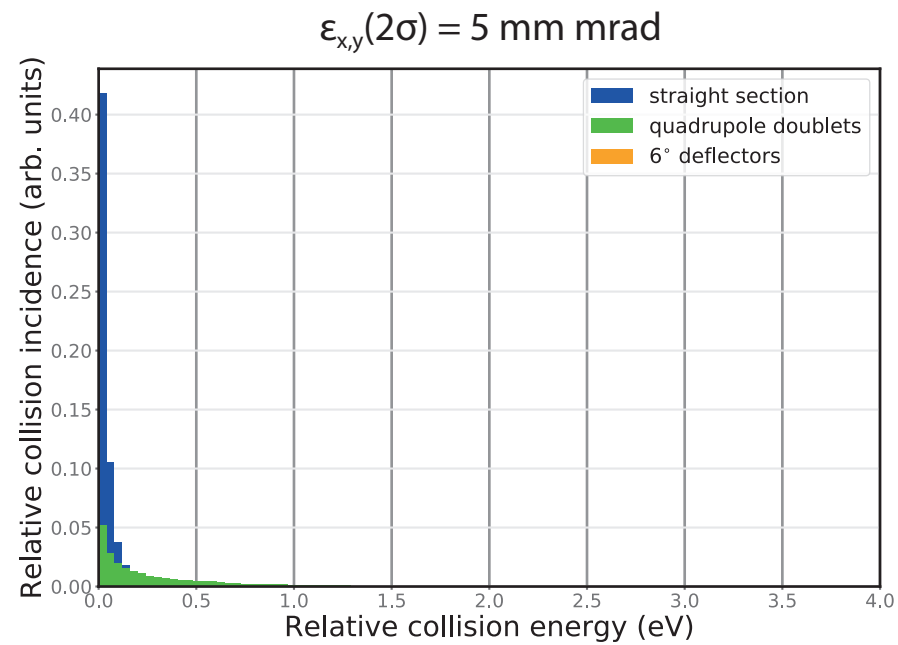
$\varepsilon_{x,y}(2\sigma) = 5$ mm mrad
straight section
quadrupole doublets
6° deflectors
Relative collision incidence (arb. units)
Relative collision energy (eV)

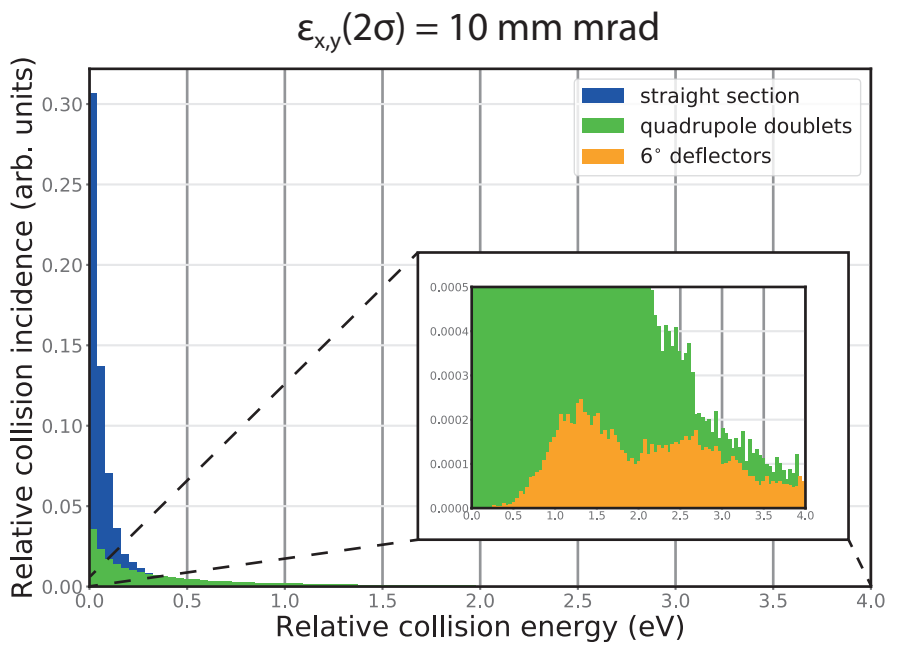
$\varepsilon_{x,y}(2\sigma) = 10$ mm mrad
straight section
quadrupole doublets
6° deflectors
Relative collision incidence (arb. units)
Relative collision energy (eV)

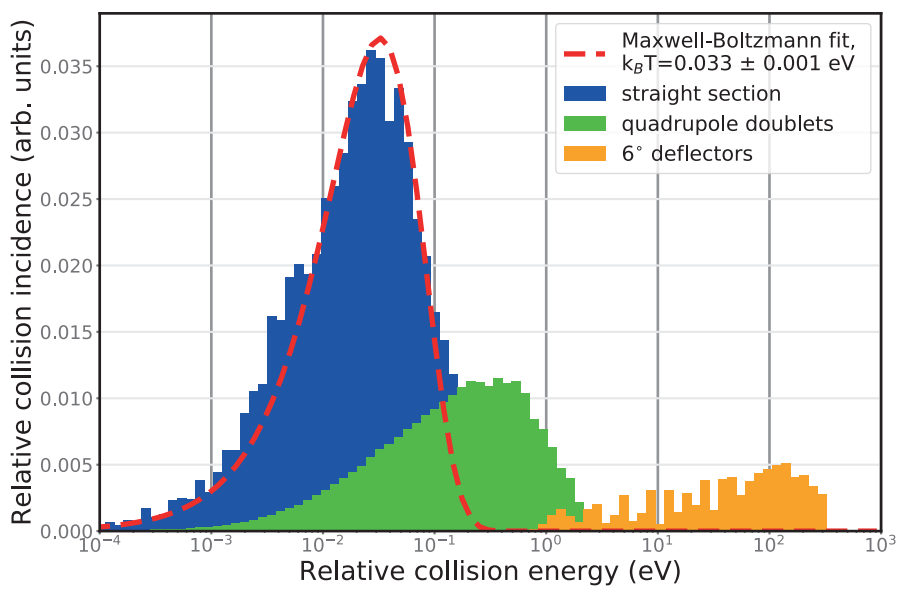
Maxwell-Boltzmann fit,
$k_B T$=0.033 ± 0.001 eV
straight section
quadrupole doublets
6° deflectors
Relative collision incidence (arb. units)
Relative collision energy (eV)

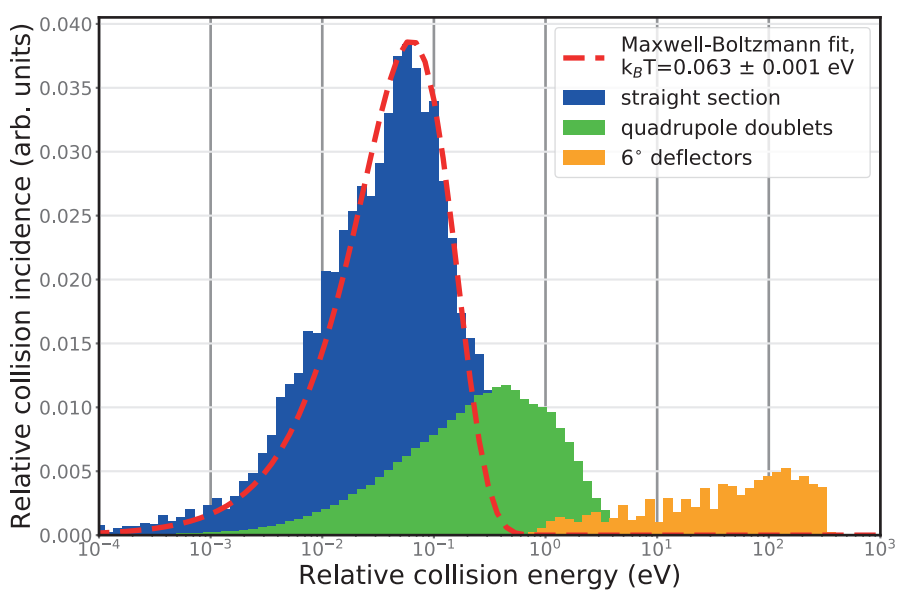
Maxwell-Boltzmann fit,
$k_B T$=0.063 ± 0.001 eV
straight section
quadrupole doublets
6° deflectors
Relative collision incidence (arb. units)
Relative collision energy (eV)

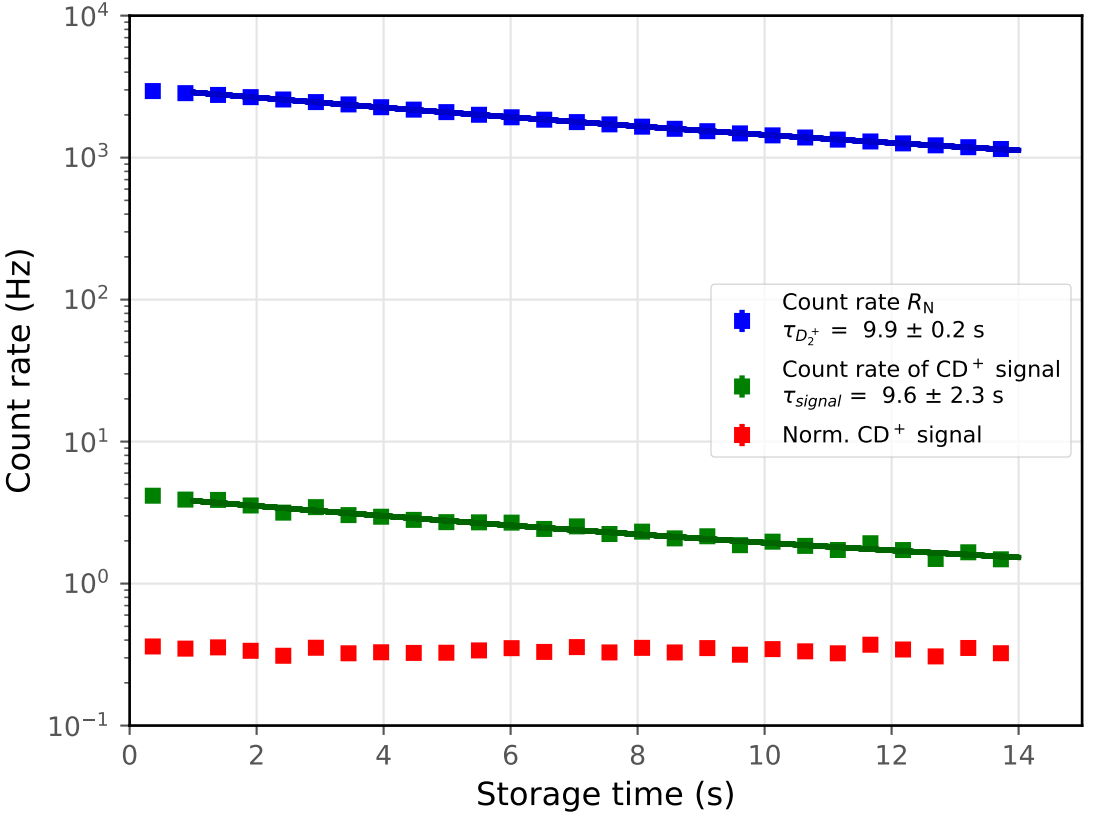
Count rate (Hz)
Storage time (s)
Count rate R_N
$\tau_{D_2^+}$ = 9.9 ± 0.2 s
Count rate of CD^+ signal
τ_{signal} = 9.6 ± 2.3 s
Norm. CD^+ signal

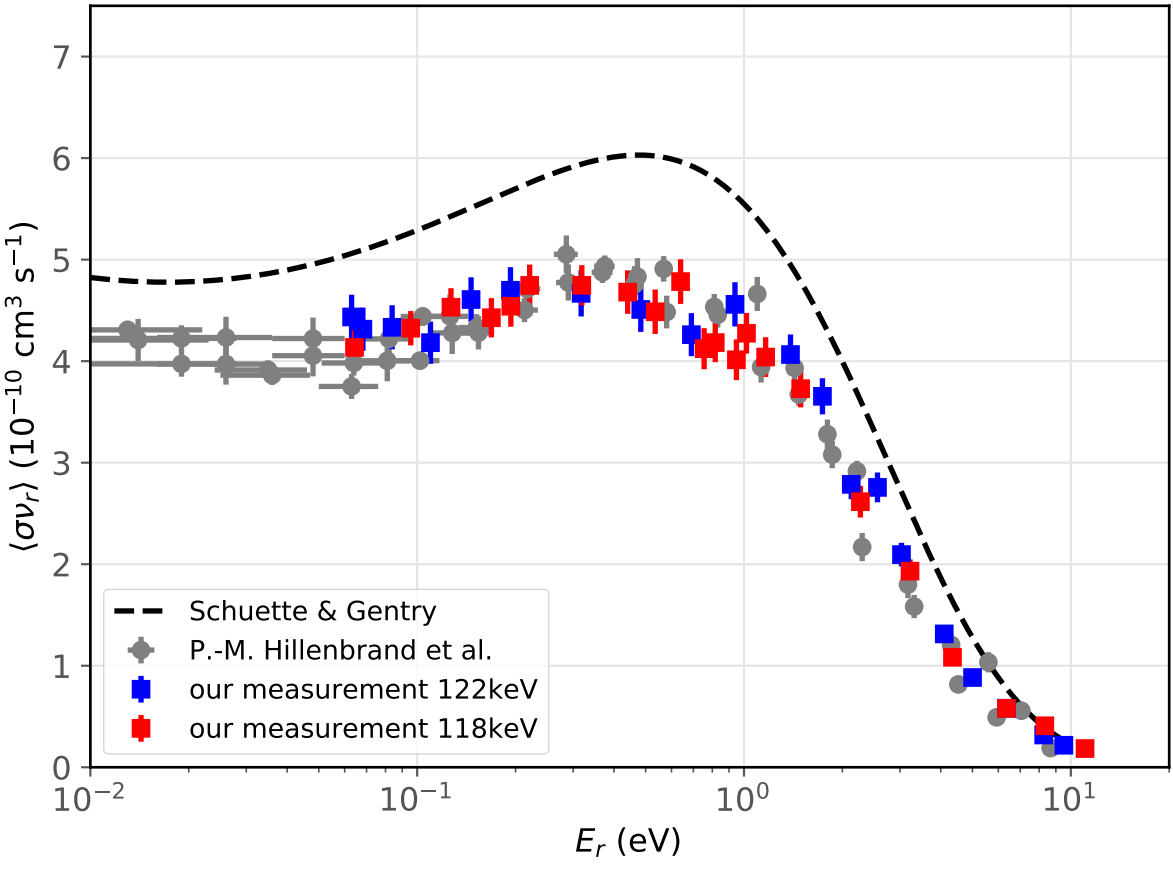
Schuette & Gentry
P.-M. Hillenbrand et al.
our measurement 122keV
our measurement 118keV
$\langle \sigma v_r \rangle$ (10^{-10} cm^3 s^{-1})
E_r (eV)
0
1
2
3
4
5
6
7
10^{-2}
10^{-1}
10^{0}
10^{1}